1-1-2008

Solution of Heat Transfer and Fluid Flow problems using meshless Radial Basis Function method

Nagamani Devi Kalla
University of Nevada, Las Vegas

SOLUTION OF HEAT TRANSFER AND FLUID FLOW PROBLEMS USING MESHLESS RADIAL BASIS FUNCTION METHOD

by

Nagamani Devi Kalla

Bachelor of Engineering in Mechanical Engineering
Nagarjuna University, India
2001

A thesis submitted in partial fulfillment
of the requirements for the

Master of Science Degree in Mechanical Engineering
Department of Mechanical Engineering
Howard R. Hughes College of Engineering

Graduate College
University of Nevada, Las Vegas
May 2008

UNLV
UNIVERSITY OF NEVADA LAS VEGAS

Thesis Approval

The Graduate College
University of Nevada, Las Vegas

November 16, 2007

The Thesis prepared by

Nagamani Devi Kalla

Entitled

Solution of Heat Transfer and Fluid Flow Problems Using Meshless Radial Basis Function Method

is approved in partial fulfillment of the requirements for the degree of

Master of Science in Mechanical Engineering

Darrell W. Pepper
Examination Committee Chair

Dean of the Graduate College

Examination Committee Member

William Culbreth
Examination Committee Member

Graduate College Faculty Representative

1017-53

ABSTRACT

Solution of Heat Transfer and Fluid Flow Problems Using Meshless Radial Basis Function Method

by

Nagamani Devi Kalla

Dr. Darrell Pepper, Examination Committee Chair
Professor, Department of Mechanical Engineering
University of Nevada, Las Vegas

In the past, the world of numerical solutions for Heat Transfer and Fluid Flow problems has been dominated by Finite Element Method, Finite Difference Method, Finite Volume Method, and more recently the Boundary Element Method. These methods revolve around using a mesh or grid to solve problems. However, problems with irregular boundaries and domains can be difficult to properly discretize.

In this thesis, heat transfer and fluid flow problems are solved using Radial Basis Functions. This method is meshless, easy to understand, and even easier to implement. Radial Basis Functions are used to solve lid-driven cavity flow, natural convection in a square enclosure, flow with forced convection over backward facing step and flow over an airfoil. Codes are developed using MATLAB. The results are compared with COMSOL and FLUENT, two popular commercial codes widely used. COMSOL is a finite element model while FLUENT is a finite volume-based code.

TABLE OF CONTENTS

ABSTRACT..... iii

LIST OF FIGURES..... vi

ACKNOWLEDGEMENTS..... viii

CHAPTER 1 INTRODUCTION..... 1
1.1 Meshless Methods..... 1
1.2 Meshless Solvers using Radial Basis Functions..... 4
1.3 Thesis Outline..... 6

CHAPTER 2 RADIAL BASIS FUNCTIONS..... 8
2.1 The RBF Method..... 8
2.2 Development of the Multiquadric Method..... 11
2.3 Shape parameter c in MQ-RBF Method..... 14

CHAPTER 3 INTERPOLATION AND APPROXIMATION..... 16
3.1 Positive Definite vs. Conditionally Positive Definite..... 17
3.2 General Methods for Interpolation and Approximation..... 19

CHAPTER 4 SOLUTION PROCEDURE..... 21
4.1 Governing Equations..... 21
4.2 Numerical Examples..... 22
4.2.1 Lid-Driven Square Cavity Flow..... 22
4.2.2 Natural Convection in a Square Enclosure..... 23
4.2.3 Flow with Forced Convection over a Backward Facing Step..... 25
4.2.4 Flow over an Airfoil..... 26
4.3 Methodology..... 27

CHAPTER 5 RESULTS AND DISCUSSION..... 32
5.1 Lid-Driven Cavity Flow..... 32
5.2 Natural Convection in a Square Enclosure..... 37
5.3 Flow with Forced Convection over a Backward Facing Step..... 42
5.4 Flow over an Airfoil..... 47

CHAPTER 6 CONCLUSIONS AND FUTURE WORK.....50
6.1 Conclusions.....50
6.2 Future Work.....51

REFERENCES.....53

VITA.....60

LIST OF FIGURES

Figure 3.1 2D representation of distances among n centers....16
Figure 4.1 Lid driven flow in a square cavity....23
Figure 4.2 Natural convection in a square enclosure....24
Figure 4.3 Problem configuration for flow over a backward facing step....26
Figure 4.4 Problem configuration for flow over an airfoil....27
Figure 4.5 Calculation Flow Chart....31
Figure 5.1 Lid driven flow in a square cavity....32
Figure 5.2 Nodal distributions for lid driven flow (a) Uniform distribution and (b) Random distribution....33
Figure 5.3 Velocity profiles for different nodal distributions (Re = 400)....34
Figure 5.4 Meshes for lid driven flow (a) COMSOL mesh (1596 nodes) (b) FLUENT 31x31 mesh....35
Figure 5.5 Velocity vectors for flow in a driven cavity using (a) Meshless (b) COMSOL (c) FLUENT....35
Figure 5.6 Velocity profiles along vertical and horizontal central lines (Re = 100)...36
Figure 5.7 Velocity profiles along vertical and horizontal central lines (Re = 400)...36
Figure 5.8 Velocity profiles along vertical and horizontal central lines (Re = 1000)..37
Figure 5.9 Natural convection in a square enclosure....37
Figure 5.10 Nodal distribution for Natural convection in a square cavity....38
Figure 5.11 Meshes for Natural Convection (a) COMSOL mesh (1596 nodes) (b) FLUENT 31x31 mesh....39
Figure 5.12 Velocity vectors using (a) Meshless (B) COMSOL (c) FLUENT ($Ra = 10^3$)....39
Figure 5.13 Velocity profiles along vertical and horizontal central lines ($Ra = 10^3$)....40
Figure 5.14 Velocity profiles along vertical and horizontal central lines ($Ra = 10^4$)....40
Figure 5.15 Velocity profiles along vertical and horizontal central lines ($Ra = 10^5$)....41
Figure 5.16 Isotherms for Natural convection in a square cavity for $Ra = 10^4$ using (a) Meshless (b) COMSOL (c) FLUENT....41
Figure 5.17 Problem configuration for flow over a backward facing step....42
Figure 5.18 Distribution of 284 nodes for flow over backward facing step....43
Figure 5.19 Meshes for backward facing step solution (a) COMSOL mesh of 388 elements (b) FLUENT mesh of 284 nodes....43
Figure 5.20 Velocity vectors for backward facing step using (a) Meshless (b) COMSOL (c) FLUENT....44
Figure 5.21 Velocity profiles for Re=800 at x=7....45
Figure 5.22 Velocity profiles for Re=800 at x=15....45
Figure 5.23 Temperature profiles for Re=800 at x=7....46
Figure 5.24 Temperature profiles for Re=800 at x=15....46

Figure 5.25 Isotherms for backward facing step using (a) Meshless (b) COMSOL (c) FLUENT.....47
Figure 5.26 Problem configuration for flow over an airfoil.....48
Figure 5.27 Distribution of 236 nodes in a rectangular domain.....48
Figure 5.28 Meshes for flow over an airfoil (a) COMSOL mesh of 2535 elements (b) FLUENT mesh of 1893 nodes.....49
Figure 5.29 Velocity vectors for flow over an airfoil using (a) Meshless (b) COMSOL (c) FLUENT.....49

ACKNOWLEDGEMENTS

I express my sincere gratitude to Dr. Darrell Pepper for his continuous guidance, support and encouragement throughout this research activity.

I would like to thank Dr. William Culbreth, Dr. Daniel Cook and Dr. Rama Venkat for their time in reviewing the prospectus, participation of defense as the committee members.

Finally, I would like to thank my parents and friends without their continuous support and faith this work would not have been possible.

CHAPTER 1

INTRODUCTION

1.1 Meshless Methods

The most commonly used approximate methods for solving the system of partial differential equations (PDEs) in fluid flow problems are the finite difference method (FDM), finite volume method (FVM) and the finite element method (FEM). Other methods also becoming more widely used include the spectral method (SM) and boundary element method (BEM). These methods have been used to solve numerous thermal related problems covering a wide range of applications.

There are some substantial difficulties in applying these techniques to realistic, geometrically complex three dimensional problems. The major problem is in creating a suitable mesh. For a complex configuration, generation of a good quality mesh can be very expensive in terms of human labor and CPU time. Meshing is often the most time consuming part of the solution process and is far from being fully automated. For practical problems the geometries encountered can be highly irregular. Hence it would be desirable to be able to solve partial differential equations (PDEs) over irregular domains without having to discretize the domains.

To avoid discretization, a number of numerical schemes have been proposed in the past two decades which are referred to as gridless or meshless schemes. They are also known as meshfree methods. In the sequel the terms gridless, meshless and meshfree

will be used synonymously. These schemes completely discard the idea of a mesh for the spatial discretization of the governing partial differential equations. The meshfree term implies there is no dependence on a mesh, but such schemes can be applied to any kind of mesh-structured, unstructured or hybrid.

In the rapidly developing branch of meshfree numerical methods, there is no need to create a polygonisation, neither in the domain nor on its boundary, and represents a promising technique to avoid meshing problems [1,2,3]. A number of mesh reduction techniques such as the dual reciprocity boundary element method [4], meshfree techniques such as the dual reciprocity method of fundamental solutions [5], and meshfree local Petrov Galerkin methods (MLPG) [1,6] have been developed for transport phenomena and solution of the Navier-Stokes equations. This thesis focuses on the simplest class of mesh-free methods being employed today known as Radial Basis Function [7] methods.

A common feature of meshless methods is that neither domain nor surface polygonisation is required during the solution process. These methods are designed to handle problems with large deformation, moving boundaries, and complicated geometry. Recently, advances in the development and application of meshless techniques show they can be strong competitors to the more classical FDM/FVM/FEM approaches [8,9], and may likely become a dominant numerical method for solving science and engineering problems in the 21^{st} century.

Liu [10] discusses meshfree methods, implementations, algorithms, and coding issues for stress-strain problems. Liu [10] also includes Mfree2D, an adaptive stress analysis software package available for free from the web. Atluri and Shen [1] produced research

monograph that describes the meshless method in detail, including much in-depth mathematical basis. They also present comparison results with other schemes.

Meshless methods are an attempt to minimize mesh dependence problems in computational methods. The objective is to eliminate at least part of this mesh dependence by constructing the approximation entirely in terms of nodes. Moving discontinuities can usually be treated without remeshing with only a slight compromise with accuracy. Large scale problems can be solved using meshless methods with comparable accuracy and more efficiently than conventional mesh based schemes. The nodes can be created in a fully automated manner without any human intervention and hence the time spent in mesh generation is saved [10].

The origin of meshless methods can be traced back to the 1970's, but very little research was done until the past decade. The starting point, which seems to have the longest history, is the smooth particle hydrodynamics (SPH) method (Lucy, 1977) [11], which was used for modeling astrophysical phenomenon. One of the common characteristics of all the meshfree methods is that a functional approximation or interpolation can be constructed from a set of scattered nodes or points. These methods do not require any storage of prespecified connectivity or relationship among the scattered nodes.

One of the main advantages of meshless methods is that they are computationally easy to add or remove nodes from a preexisting set of nodes. In conventional FDM, FVM, FEM and BEM [12] methods, addition or removal of a point or an element may lead to lengthy remeshing and is usually difficult to implement. Radial basis functions are the natural generalization of univariate polynomial splines to a multivariate setting. The main

advantage of this type of approximation is that it works for arbitrary geometry with high dimensions and does not require any mesh. A RBF is a function whose value depends only on the distance from some center point. Using distance functions, RBFs can be easily implemented to reconstruct a plane or surface using scattered data in 2-D, 3-D or higher dimensional spaces.

Meshless methods hold promising alternative approaches for problems involving fluid flow and heat transfer analysis. The lack of a mesh that is required in the more conventional numerical approaches becomes particularly advantageous in that one can easily refine (or adapt as a mesh-based technique) for CFD problems.

1.2 Meshless Solvers using Radial Basis Functions

In the past decade researches have been developing meshless methods based on the use of radial basis functions (RBFs) for solving partial differential equations (PDEs). The idea of using radial basis functions for solving PDEs was first proposed by Kansa (1990), where a global multiquadric scheme was used in conjunction with point collocation to discretize parabolic, hyperbolic and elliptic PDEs.

Radial basis functions have wide applications in sciences and mathematics where a function is to be approximated or interpolation is needed. For example, in thin plate splines (TPSs) RBFs are used for mapping images such as underwater sonar scans into other images for comparison – in such cases interpolation comes into play. Another category of RBFs called multiquadrics have very good performance when dealing with interpolation problems like potential or temperature. Multiquadrics have been useful in

atmospheric studies where the temperature is known at scattered meteorological stations on the earth's surface.

RBF methods rely on a set of random points, rather than a set of grid points defined at mesh intersections, to discretize the PDEs and the field variables. For certain values of RBF widths, the methods are capable of giving very accurate results and make them very attractive. RBF methods have found applications in many branches of computational engineering, for example, in heat transfer [13], fluid flow [14], solid mechanics, micro-electrical-mechanical system [15] and electromagnetism. Mai-Duy and Tran-Cong [16] proposed an indirect RBF method, which is based on integration rather than differentiation for approximating functions and their derivatives and for solving elliptic differential equations.

In Kansa's method [3], a function is first approximated by an RBF, and its derivatives are then obtained by differentiating the RBF. In the indirect RBF method, on the other hand, the highest order derivatives in the system under consideration are first decomposed into RBFs. Lower order derivatives and the function itself are then successfully obtained via symbolic integrations. Mai-Cao and Tran-Cong [17] extended the indirect RBF method for solving transient problems governed by parabolic, hyperbolic and convection-diffusion equations. Although RBFs were initially developed for multivariate data and function interpolation, their truly meshfree nature has motivated researchers to employ them in solving PDEs, especially for higher dimension problems.

The most credit for using RBFs to solve PDEs goes to Kansa [3], who discretized PDEs directly over unstructured nodes using RBFs. Though his approach was similar to the finite difference method (FDM), it was suitable for any scattered distribution of nodes.

He has also given a historical perspective on the development of meshfree methods and their application in various fields of computational science and engineering [18]. Other contributions in the area of RBFs comes from Fornberg [19], Chen [20] and Tanaka, including applications such as structures [21], fluid dynamics [22] and fluid structure interaction [23].

RBFs when used as basis functions for multi-variate data interpolation, show favorable properties like high efficiency and good quality. There are two main advantages of using RBFs to solve PDEs. One is that they are naturally mesh-free which means they have the ability to handle scattered data. The second advantage is that they have higher-order accuracy than typical finite difference schemes on a scattered distribution of nodes.

1.3 Thesis Outline

This thesis is focused on the simplest class of mesh-free methods in development today - the Radial Basis function methods. The fluid flow problem is generally a global problem. In order to solve a global problem one needs to solve a global matrix [24]. Solving matrices for global systems with a fine mesh grid or simulating complex geometries can become difficult. Therefore, a completely local scheme for solving fluid flow problems is proposed.

A common approach is to solve the pressure poisson equation or/and pressure correction Poisson equation [25]. A much simplified local pressure-velocity coupling (LPVC) algorithm is proposed. The proposed algorithm is tested on a set of classical benchmark problemS analysed by Gartling [51] and De Vahl Davis [26] for heat transfer

and fluid flow problems. The method represents a local variant of an already developed global solution [27] for coupled heat transfer and fluid flow problems. This local variant was developed for diffusion problems [28], convection-diffusion solid-liquid phase change problems [29] and successfully applied in the industrial process of direct chill casting [30]. In this thesis the spectra of physics is extended to the solution of coupled mass, energy and momentum equations.

CHAPTER 2

RADIAL BASIS FUNCTION

2.1 The RBF Method

Radial basis functions (RBFs) are increasingly being used as an alternative to traditional discretization schems employed in finite difference, finite volume, and finite element methods. RBF based methods have several attractive features, most notably fast convergence (exponential for some cases) and the flexibility in the choice of node location; in fact some implementations do not require an underlying grid or mesh. For this reason they are called meshfree numerical schemes. A major advantage with using RBFs is that the points on the grid do not need to be uniform in anyway. A random scattering of data points can be used just as easily as a uniform grid.

A radial basis function in two dimensions is defined as follows:

$$\phi : R^2 \longrightarrow R$$

$$\phi(x,y) = f(\|(x,y)-(x_i,y_i)\|)$$

The distance between points (x,y) and point (x_i, y_i) is denoted as follows:

$$r = \|(x,y)-(x_i,y_i)\|$$

There are many RBFs which have been suggested and applied in various numerical schemes. The most commonly used RBFs are

Multiquadrics (MQs): $\phi(r) = \sqrt{r^2 + c^2}$, c > 0,

Thin-Plate Splines (TPS): $\phi(r) = r^2 \log(r)$,

Gaussians: $\phi(r) = e^{-\alpha r^2}$, $\alpha > 0$,

Inverse MQs: $\phi(r) = 1/\sqrt{r^2 + c^2}$, c > 0,

The c parameter in the multiquadric and inverse multiquadric functions is a shape parameter represented as a positive real number (discussed later). A way of thinking about RBFs is that they are an enhanced metric that describes the distances between points in a way that is more suitable with PDEs.

Among the above RBFs the first one, MQs are most extensively used and were proposed by Hardy [33]. Franke [34] studied RBFs and found that MQs generally perform better than others for the interpolation of 2D scattered data. The exponential convergence of MQ makes it superior to other RBFs such as thin plate splines (TPS). In the present work we will be using and presenting the MQ RBFs.

The RBF method is an ideal tool for interpolating multidimensional scattered data. Its simple form, and ability to accurately approximate an underlying function, have made the method particularly popular. The types of $\phi(r)$ available for use in the RBF method can be split into two main categories: (1) infinitely smooth and (2) piecewise smooth. The infinitely smooth function features a shape parameter c, such that as $c \longrightarrow 0$ the basis functions become increasingly flat. When considering the accuracy of the RBF interpolants and the stability of the corresponding linear system, two very different

situations arise. These two situations are determined by whether the $\phi(r)$ used in the method is piecewise smooth or infinitely smooth.

For the piecewise smooth case, as the number of data points increases in a fixed domain, the RBF interpolants converge algebraically to the underlying (sufficiently smooth) function being interpolated. The rate of convergence is directly related to the smoothness of $\phi(r)$ [31], and the rate often increases as the number of space dimensions increases. The stability of the linear system for the piecewise smooth case is also related to the amount of smoothness of $\phi(r)$ [32].

A very important feature of the RBF method is that its complexity does not increase as dimension of the interpolation increases (apart, of course, from the trivial change of computing distances in higher dimensions). Their simple form makes implementing the methods extremely easy (compared to, for example, a cubic spline method). However, three main computational challenges exist:

(a) The matrix for determining the interpolation coefficients is dense, which makes the computational cost of the methods high.

(b) The matrix is ill-conditioned when the number of data points is large.

(c) For the infinitely smooth RBFs and a fixed number of data points, the matrix is also ill-conditioned when c is small.

Most of the studies devoted to resolving (a) also provide some preconditioning techniques for resolving (b).

2.2 Development of the Multiquadric Method

The RBF method is a generalized version of the multiquadric (MQ) method developed in 1968 by Hardy [33]. Hardy developed the MQ method to solve a problem from cartography. Namely, given a set of sparse, scattered measurements from some source points on a topological surface (e.g. elevation measurements from Rocky Mountain National park), construct a "satisfactory" continuous function that represents the surface. Here satisfactory means a function that provides an exact fit of the data and provides good approximation of the features of the surface.

Hardy's first step was to study a one dimensional version of the problem, namely construct a satisfactory function that represents a topographic profile (a curve) from scattered measurements of the profile. While studying the problem, he found that the profile could be represented fairly satisfactorily by a piecewise linear interpolating function. For a set of n distinct (scattered) source points $\{x_j\}_{j=1}^n$ and corresponding measurements $\{f_j\}_{j=1}^n$, he proposed the following form for the interpolation function:

$$s(x) = \sum_{j=1}^{n} \lambda_j |x - x_j| \tag{2.1}$$

The problem with representing a topographic profile is that the function has a jump in the first derivative at each data point. Hardy realized that this problem could be easily resolved by replacing the absolute value basis function by one that is continuously differentiable. He proposed using the basis function $(c^2+x^2)^{1/2}$, where c is some non-zero arbitrary constant, because of its similarity to the absolute value function. The new interpolating function thus becomes

$$s(x) = \sum_{j=1}^{n} \lambda_j \sqrt{c^2 + (x - x_j)^2} \tag{2.2}$$

Hardy found that this new method not only provided an accurate representation of a topographic profile, but that the techniques of calculus could be easily applied to it. The key property with Hardy's approach was that it carries over to more than one dimension. The absolute value of the difference between two one-dimensional points is simply the Euclidean distance between the points. The natural extension to two dimensions is to create an interpolating function based on translates of the Euclidean distance function in two dimensions. Hardy proposed interpolating the data with the function,

$$s(x, y) = \sum_{j=1}^{n} \lambda_j \sqrt{(x - x_j)^2 + (y - y_j)^2} \tag{2.3}$$

Geometrically, this method corresponds to interpolating the data by a linear combination of n translates of a cone (i.e. a radially symmetric function $\varphi(r) = r$, where $r = \sqrt{x^2 + y^2}$). The vertex of each cone is centered at one of the source points. Like its one dimensional equivalent, this new two-dimensional method suffers from the problem that it results in a piecewise continuous function. Also like its one-dimensional equivalent, Hardy was able to find a simple solution to alleviate the problem. Instead of using a linear combination of the Euclidean distance basis function to interpolate the data, he again proposed using a linear combination circular hyperboloid basis functions (i.e. rotated hyperbola basis functions $(c^2+x^2)^{1/2}$), translated to be centered at each source point. The exact form of this new type of interpolant is given by

$$s(x, y) = \sum_{j=1}^{n} \lambda_j \sqrt{c^2 + (x - x_j)^2 + (y - y_j)^2} \tag{2.4}$$

For $c \neq 0$, this function is infinitely differentiable, thus techniques in multivariable calculus can be used for determining properties of the topographic surface which the function is approximating.

This method did not suffer from large oscillations like Fourier series methods and was able to account for rapid variations of the topographic surface unlike the polynomial series methods. Hardy named this technique the "multiquadric method" because he considered the principal feature of the method to be a "superpositioning of quadric surfaces".

While Hardy originally developed the MQ method for solving the two-dimensional interpolation problem, he realized that it could be easily generalized for interpolating data in any dimension. A three-dimensional interpolation method is then easily created by having the basis function only depend on the distance of the point (x,y,z) from its center (x_i,y_i,z_i).

One of the most important studies of the MQ method was done in 1979 by Franke [34]. This study was primarily concerned with investigating a vast number of the available methods for interpolating two-dimensional scattered data in order to determine which methods deserved further mathematical study. Although Franke provided empirical evidence that the MQ method deserved more attention, he also expressed some reservations about the method. A mathematical foundation of the MQ method was ultimately provided in 1986 by Micchelli [35]. Besides providing a proof of Franke's conjecture, Micchelli provided sufficient conditions to guarantee the nonsingularity of the method when a number of other basis functions are used. The MQ method was recognized as only one specific example of a more general method.

2.3 Shape parameter c in MQ-RBF method

The shape parameter c strongly influences the accuracy of the MQ-RBF method. The key factor in obtaining accurate results by RBF method is the MQ matrix. The choice of the shape parameter c has been a topic of discussion in the community of RBF researchers. Franke [36] evaluated a large number of interpolation schemes in two dimensions and found that the most accurate schemes were MQ and TPS. He suggested a formula to find the optimum shape parameter c as

$$c = \frac{1.25 * D}{\sqrt{N_I}} \tag{2.5}$$

where D is the radius of the smallest circle and N_I is the number of nodes in the support domain.

Hardy [33] suggested another formula for evaluating the shape parameter c.

Hardy: c= 0.815d

where, $d = \frac{1}{N_I} \sum_{i=1}^{N_I} d_i$

d_i is the distance between the i^{th} data point and its nearest neighbor.

The behavior of the function to be interpolated has an important role in determining the optimal value of the shape parameter. A small value of c can be used if the function is rapidly varying and a large value if the function is smooth (has large curvature). The root mean squared errors of many of the bivariate functions were reduced when the optimal shape parameter was used [37]. The method of cross validation can be used to estimate the optimal shape parameter of elliptic PDE problems in two and three dimensions and observed exponential convergence.

A general theoretical analysis of how the shape parameter c is associated with the accuracy of approximation is difficult. In this work utilizing numerical experimentation on functions of two variables, it was found there is an optimum value of c at which the accuracy of the scheme is a maximum and remains constant over a range of c. But after a critical value of c is reached, the error increases infinitely. The choice of c within a domain ensures best approximation. A similar trend is observed for both the first and higher order derivatives.

CHAPTER 3

INTERPOLATION AND APPROXIMATION

RBFs work by interpolating a known function *f* from a set of n data points. These data points are known as interpolation points. Given a 2D finite set of scattered n data points (x_i,y_i), often known as centers (or interpolation points), it is assumed that some function values $f(x_i,y_i)$ are known. Based on this known data, the task is to approximate a function that will fit the function values. Using RBFs, one can find a linear combination that closely approximates the function *f*:

$$f(x,y) = \hat{f}(x,y) \tag{3.1}$$

$$\hat{f}(x,y) = \sum_{i=1}^{n} \alpha_i \phi(x,y)$$

(3.2)

$$\phi(x,y) = \phi(r), r = \sqrt{(x-x_i)^2 + (y-y_i)^2} \tag{3.3}$$

where $\{\alpha_i\}$ are unknown coefficients that are to be determined.

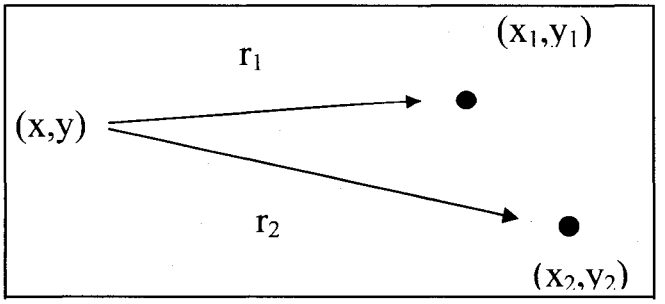

Figure 3.1. 2D representation of distances among n centers (n=3)

These distances are then applied to a selected radial basis function and written as n linear combination equations. The resulting system is

$$A\bar{\alpha} = \bar{f}\,, \tag{3.4}$$

where A is the n x n symmetric coefficient matrix of the linear equations, $\bar{\alpha}$ is the vector of corresponding unknown coefficients, and $\bar{f}$ is a vector of the associated function values. Provided matrix A is nonsingular, the unknown coefficients $\{\alpha_i\}$ are uniquely solvable:

$$\bar{\alpha} = A^{-1}\bar{f} \tag{3.5}$$

3.1 Positive Definite vs. Conditionally Positive Definite

The nonsingular condition of the interpolation matrix A is a critical issue when attempting to solve for the unknown coefficients $\{\alpha_i\}$. If the matrix is positive definite, then it is non singular and invertible. Selecting RBFs denoted with a conditionally positive definite (CPD) order of zero will ensure that the matrix is positive definite. Hence, RBFs with CPD order of zero are called symmetric positive definite (SPD).

For RBFs with a CPD order of m (e.g., the TPS or cubic spline), the nonsingular condition of matrix A is not met. Fortunately, this can be overcome by the addition of polynomial terms. In this case, such RBFs are called conditionally positive definite (CPD) with order m. The approximation of function f then becomes

$$\hat{f}(x,y) = \sum_{i=1}^{n} \alpha_i \phi_i(r) + \sum_{j=1}^{M} \alpha_j P_j(x), \tag{3.6}$$

along with the constraints

$$\sum_{i=1}^{n} \alpha_i P_j(x_i) = 0, \quad 1 \leq j \leq M, \tag{3.7}$$

For example, if $\phi(r) = r^2 \log r$ were chosen as the RBF, then M=3, and the function f would be approximated by n+3 equations:

$$\hat{f}(x,y) = \sum_{i=1}^{n} \alpha_i r^2 \log r + \alpha_{n+1} + \alpha_{n+2} x + \alpha_{n+3} y, \tag{3.8}$$

with the constraints

$$\sum_{i=1}^{n} \alpha_i = \sum_{i=1}^{n} \alpha_i x_i = \sum_{i=1}^{n} \alpha_i y_i = 0$$

The eigenvalues and condition number of matrix A are also significant issues in the RBF approximation. If A is an n x n matrix, then any scalar λ satisfying the equation

$$Ax = \lambda x, \tag{3.9}$$

for some m x 1 vector $x \neq 0$, is called an eigenvalue of A. The matrix A can have many eigenvalues. The condition number of A is given by

$$\text{cond}(A) = \lambda_{max}/\lambda_{min}, \tag{3.10}$$

where λ_{max} and λ_{min} are the maximum and minimum eigen values of A.

The condition number indicates the sensitivity of the solution. Very large condition numbers indicate an ill-conditioned problem and unreliable solution, while small condition numbers point toward solution stability. The accuracy of the RBF is inversely related to the condition number of the interpolation matrix.

3.2 General Methods for Interpolation and Approximation

The most frequently employed techniques for multivariate approximation, other than radial basis functions, are straight polynomial interpolation, and piecewise polynomial

splines. There are various highly specific techniques for forming polynomial interpolants. Very special considerations are needed because as long as a finite generic set of data sites from an open set in more than one dimension, and if we are interpolating from a polynomial space independent of finite generic set of data sites, there can always be singularity of the interpolation problem.

A completely different approach for polynomial interpolation in several unknowns is divided differences represented in terms of simplex splines and directional derivatives to express the polynomials. The representations of the approximants are usually ill-conditioned and therefore not too useful in practical applications.

Spline, i.e. piecewise polynomial, methods usually require a triangulation of the set of data sites in order to define the space from which we approximate, unless the data sites are in very special positions, e.g. gridded or otherwise highly regularly distributed. The reason for this is that it has to be decided where the pieces of the piecewise polynomials lie and where they are joined together. Moreover, it then has to be decided with that smoothness they are joined together at common vertices, edges etc. and how that is done. This is not at all trivial in more than one dimension and it is highly relevant in connection with the dimension of the space.

Triangulations or similar structures (such as quadrangulations) are very difficult to provide in more than two dimensions. This is one of the severest disadvantages of piecewise polynomial techniques and a good reason for using radial basis functions (in three or more dimensions) where no triangulations are required. Moreover, the quality of the spline approximation depends severely on the triangulation itself - long and thin

triangles, for instance, often being responsible for the deterioration of the accuracy of approximation.

In summary, there are many approximation methods in several dimensions other than radial basis functions, the most attractive being usually ones that generate piecewise polynomials. However, these methods require much set-up work, especially in more than two dimensions, and is a strong argument in favor of radial basis functions.

CHAPTER 4

SOLUTION PROCEDURE

4.1 Governing Equations

Assuming incompressible laminar flow with convective heat transfer effects, the following scaling relations are used in the governing equations of momentum and energy

$$X = \frac{X^*}{L},\ V = \frac{V^*}{\alpha/L},\ p = \frac{p^*}{\rho\alpha^2/L^2},\ t = \frac{t^*}{L^2/\alpha},\ T = \frac{(T^* - T_c)}{(T_h - T_c)} \tag{4.1}$$

* represents the dimensional variables which are non dimensionalised using scaling relations.

with the Reynolds number, Rayleigh number, Prandtl number and Peclet number defined as

$$\mathrm{Re} = \frac{\rho VL}{\mu},\ Ra = \frac{g\beta(T_h - T_c)L^3}{\alpha\upsilon} \tag{4.2}$$

$$\mathrm{Pr} = \frac{\upsilon}{\alpha},\ Pe = \frac{VL}{\alpha} \tag{4.3}$$

The non-dimensional forms of the governing equations become

Conservation of Mass:

$$\nabla \cdot V = 0 \tag{4.4}$$

Conservation of Momentum:

$$\frac{\partial V}{\partial t} + V \cdot \nabla V = -\nabla p + C_{visc}\nabla^2 V + B \tag{4.5}$$

where the body force is defined as B = PrRaT in the y-direction for natural convection problems. For all the other cases, B = 0.

Conservation of Energy (neglecting source term):

$$\frac{\partial T}{\partial t} + V \cdot \nabla T = C_T \nabla^2 T \tag{4.6}$$

Table 4.1: Coefficients in the governing equations

Case	C_{visc}	C_T
2-D lid driven cavity	1/Re	N/A
Natural convection in a differentially heated enclosure	Pr	1
Flow with forced convection over backward facing step	1/Re	1/Pe
Flow over an air foil	1/Re	N/A

4.2 Numerical Examples

4.2.1 Lid-Driven Square Cavity flow

The lid-driven cavity is one of the most frequently employed benchmark cases to evaluate accuracy and feasibility of numerical algorithms and commercial CFD software. The problem looks simple in many ways, but the flow in a cavity retains all the flow physics with counter rotating vortices appearing in the corners of the cavity as Re increases. Many papers are available in the literature. Several studies employed systematic experiments [38-40], others employed various numerical schemes, such as vorticity-stream function FDM [41], least-square FEM [42], and projection FEM [43].

Problem definition

The boundary conditions for flow in a lid-driven cavity ($0 \leq x \leq 1$, $0 \leq y \leq 1$) with the top lid moving at a unit velocity are described as

On the top wall:

$$u = 1, v = 0$$

On all the other walls:

$$u = v = 0$$

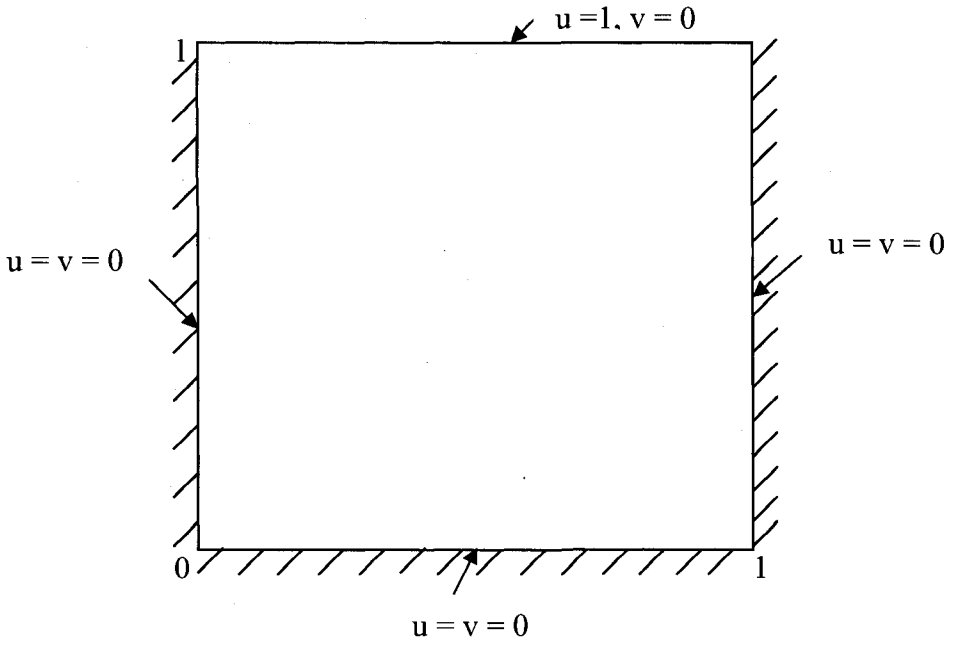

Figure 4.1. Lid driven flow in a square cavity

4.2.2 Natural Convection in a Square Enclosure

Natural convection in a square enclosure is another very popular benchmark problem which has been studied extensively over the past 30 years. Many papers continue to appear in the literature utilizing various numerical techniques [44-47]. Researchers

usually compare their simulation results with the benchmark solutions obtained by De Vahl Davis [48], who employed a finite difference scheme with a stream function/vorticity formulation.

Problem Definition

The boundary conditions for natural convection in a differentially heated square enclosure ($0 \leq x \leq 1, 0 \leq y \leq 1$) can be described as

On the hot left wall:

$$u = v = 0, T = 1$$

On the cold right wall:

$$u = v = 0, T = 0$$

On the adiabatic top and bottom wall:

$$u = v = 0, \partial T/\partial y = 0$$

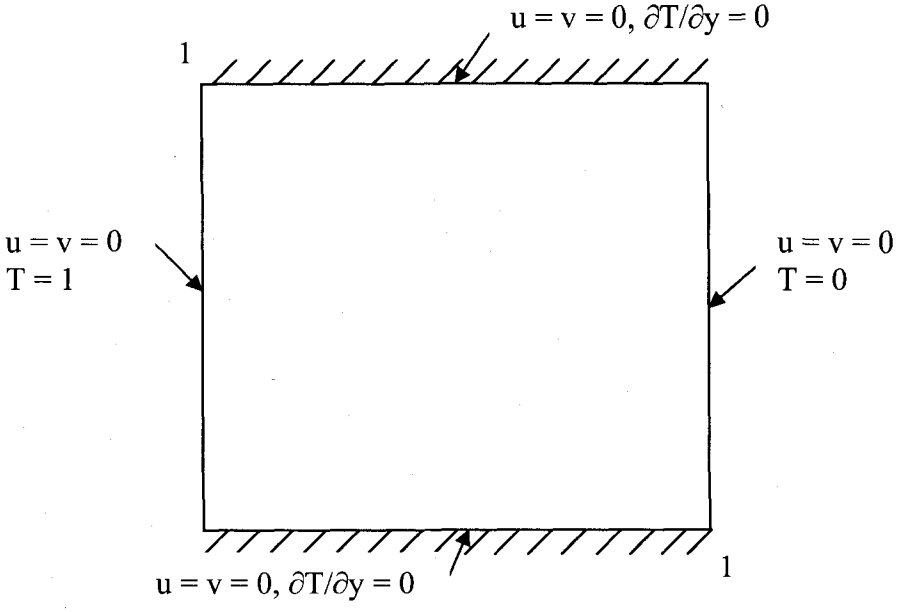

Figure 4.2. Natural convection in a square enclosure

4.2.3 Flow with forced convection over a backward facing step

Two-dimensional flow over a backward facing step is also a well known benchmark case that has been studied extensively over many years – the problem is easy to set up with known (expected) results at various Reynolds numbers. Early research work for this problem focused on the fluid pattern, and many numerical simulations for this case can be found in the literature. Gartling [51] examined this problem for assessing outflow boundary conditions. In 1992, Blackwell and Pepper [52] suggested flow over the backward facing step with heat transfer as an ASME benchmark test problem. Twelve numerical simulations were presented.

Problem definition

Figure 4.3 shows the configuration of forced convection in the 2-D backward facing step. The boundary conditions for this problem are described as

For inlet flow:

$$u(y) = \begin{cases} 0, & \text{for } 0 \le y \le \frac{1}{2} \\ 8y(1-2y), & \text{for } \frac{1}{2} < y \le 1 \end{cases}$$

$$T(y) = [1-(4y-1)^2][1-1/5(4y-1)^2] \quad \text{for } \frac{1}{2} < y \le 1$$

$$v(y) = 0$$

$$\partial T(y)/\partial x = 0 \quad \text{for } 0 \le y \le \frac{1}{2}$$

On upper and lower walls:

$$u(y) = v(y) = 0$$

$$\nabla T . \check{n} = 32/5$$

where $\check{n}$ is the outward unit vector normal to the domain boundary.

For outlet Flow:

p = 0

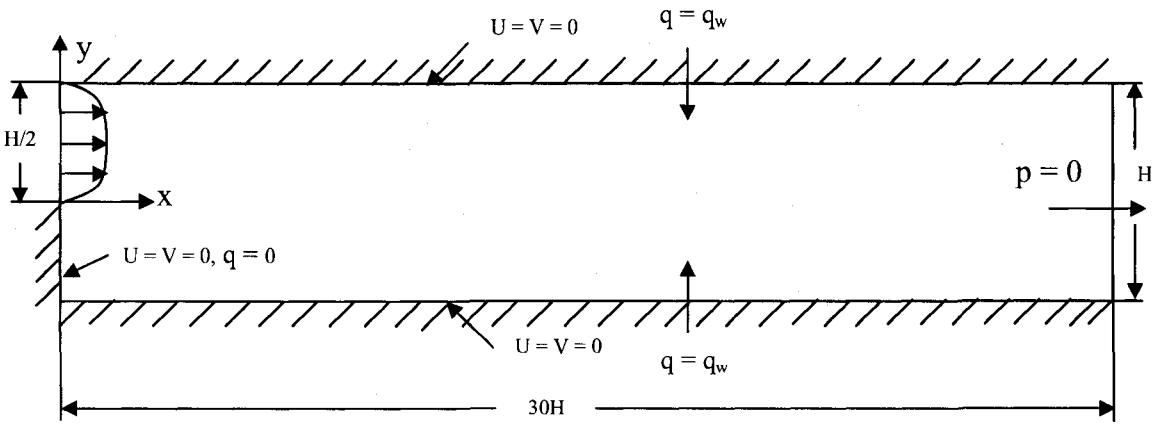

Figure 4.3. Problem configuration for forced convection in a backward facing step

4.2.4 Flow over an airfoil

Flow over an airfoil is another very popular problem which has been studied. Several studies employed systematic experiments and others employed various numerical schemes [49-50]. In this thesis, flow over a Selig S1210 which is a high lift, low Reynolds number airfoil with zero attack angle, is examined. Figure 4.4 shows the configuration of the flow over the airfoil.

Problem definition

Boundary conditions for flow over an air foil can be described as

On the left wall: u = 1, v=0

On upper and lower walls: u = 1, v=0

On right wall: p = 0

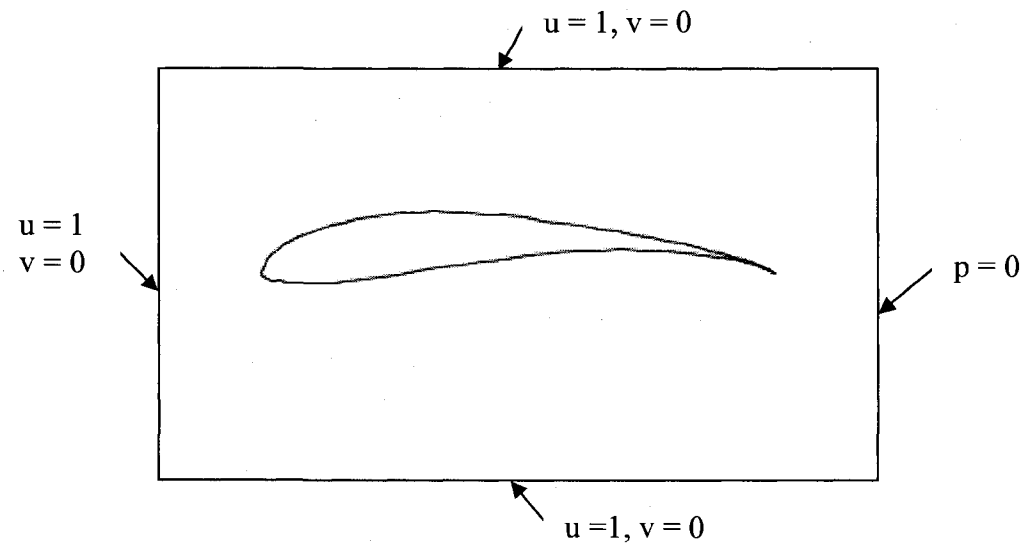

Figure 4.4. Problem configuration for flow over an airfoil

4.2 Methodology

Instead of solving a pressure Poisson equation as typically done in most numerical approaches, a simplified local pressure-velocity coupling (LPVC) algorithm is proposed. The method represents a local variant of already developed global solution, for coupled heat transfer and fluid flow problems. This local variant was already developed for diffusion problems, convection-diffusion solid-liquid phase change problems and subsequently successfully applied in industrial process of direct chill casting [28,29]. In this thesis, the spectra of physics is extended to the solution of coupled mass, energy and momentum equations. In order to solve such problems, the time dependent variant of equations are employed. An explicit time scheme using a simple finite difference approximation is adopted to calculate the time derivative. The Navier-Stokes equations are solved iteratively. The LPVC algorithm, where pressure correction is estimated from local mass continuity violation, is used to drive the intermediate velocity towards a divergence-free velocity.

In the first step the velocity is estimated from the discretized form of momentum equation. The calculated velocity $\hat{v}$ does not satisfy the mass continuity equation. In order to couple mass continuity equation and momentum equation, an iteration is used where the first iteration velocity and pressure are set to

$$\begin{aligned} v^m &= \hat{v}, \\ P^m &= P_0 \end{aligned} \qquad m = 1$$

where m denotes iteration index and P_0 denotes pressure at time t_0.

To project the velocity into the divergence free space, a correction term is added

$$\nabla \cdot (v^m + \breve{v}) = 0 \rightarrow \nabla \cdot v^m = -\nabla \cdot \breve{v} \tag{4.7}$$

where $\breve{v}$ stands for velocity correction.

Velocity correction is affected only by the effect of pressure correction, i.e.,

$$\breve{v} = -\frac{\Delta t}{\rho} \nabla \breve{P} \tag{4.8}$$

where $\breve{P}$ stands for pressure correction. The pressure correction Poisson equation is constructed by applying the divergence to the equation (4.8)

$$\nabla^2 \breve{P} = \frac{\rho}{\Delta t} \nabla \cdot v^m \tag{4.9}$$

Instead of solving equation (4.9) with the proper pressure correction boundary conditions, the pressure correction is assumed to be linearly related to the Laplacian for pressure correction. Therefore, in the second step, the pressure correction is calculated as

$$\breve{P} \approx L^2 \nabla^2 \breve{P} = L^2 \frac{\rho}{\Delta t} \nabla \cdot v^m \tag{4.10}$$

where L stands for characteristic length.

Equation (4.10) enables solving the problem locally. In the third step, the intermediate pressure and velocity are corrected as

$$P^{m+1} = P^m + \beta \breve{P}$$
$$v^{m+1} = v^m - \beta \frac{\Delta t}{\rho} \nabla \breve{P} \tag{4.11}$$

where β stands for relaxation parameter.

If the criteria

$$\nabla \cdot v^{m+1} < \varepsilon_v \tag{4.12}$$

is not met, than the iteration returns to equation (4.10), else the pressure-velocity iteration is completed. The calculation proceeds to the next step in the case of natural convection in a square enclosure and flow over a backward facing step.

In the fourth step the temperature is estimated from the discretized form of energy equation. Steady-state is achieved when the criteria (4.13) is met at all nodes. If criteria (4.8) is not met, calculation returns back to the first step.

$$\frac{|T - T_0|}{|T_0|} < \varepsilon_T \quad ; \quad T_0 \neq 0$$
$$T < \varepsilon_T \quad ; \quad T_0 = 0 \tag{4.13}$$

where T_0 and T denote temperature at time t_0 and $t_0+\Delta t$.

Discretized equations using RBFs

Since multiquadrics (MQ) are infinitely smooth functions, they are often chosen as the trial function for ϕ (some form of RBF), i.e.,

$$\phi(r_j) = \sqrt{r_j^2 + c^2} = \sqrt{(x - x_j)^2 + (y - y_j)^2 + c^2} \tag{4.14}$$

where c is a shape parameter provided by the user.

Momentum equation discretized using a linear combination of RBFs and is given by equation 4.15.

$$\sum_{j=1}^{N}\hat{V}_j^{n+1}\phi_j(x_i,y_i)=\sum_{j=1}^{N}V_j^n\phi_j(x_i,y_i)+\Delta t\left[C_{visc}\sum_{j=1}^{N}V_j^n\nabla^2\phi_j(x_i,y_i)-\sum_{j=1}^{N}P_j^n\nabla\phi_j(x_i,y_i)-\sum_{j=1}^{N}V_j^n\phi_j(x_i,y_i)\sum_{j=1}^{N}V_j^n\nabla\phi_j(x_i,y_i)+\sum_{j=1}^{N}B_j^n\phi_j(x_i,y_i)\right] \quad (4.15)$$

i = 1,2,…..,N_I

Discretized form for pressure correction and velocity correction equations given by equations 4.16 and 4.17 respectively.

$$\sum_{j=1}^{N}\breve{P}_j^{n+1}\phi_j(x_i,y_i)=\frac{L^2\rho}{\Delta t}\sum_{j=1}^{N}\hat{V}_j^n\nabla\phi_j(x_i,y_i), \quad i = 1,2,…..,N_I \quad (4.16)$$

$$\sum_{j=1}^{N}\breve{V}_j^{n+1}\phi_j(x_i,y_i)=\frac{\Delta t}{\rho}\sum_{j=1}^{N}\breve{P}_j^n\nabla\phi_j(x_i,y_i), \quad i = 1,2,…..,N_I \quad (4.17)$$

Intermediate pressure and velocity correction equations discretized and given by equations 4.18 and 4.19 respectively.

$$\sum_{j=1}^{N}P_j^{n+1}\phi_j(x_i,y_i)=\sum_{j=1}^{N}P_j^n\phi_j(x_i,y_i)+\beta\sum_{j=1}^{N}\breve{P}_j^n\phi_j(x_i,y_i), \quad i = 1,2,……,N_I \quad (4.18)$$

$$\sum_{j=1}^{N}V_j^{n+1}\phi_j(x_i,y_i)=\sum_{j=1}^{N}\hat{V}_j^n\phi_j(x_i,y_i)-\beta\frac{\Delta t}{\rho}\sum_{j=1}^{N}\breve{P}_j^n\nabla\phi_j(x_i,y_i), \quad i = 1,2,……,N_I \quad (4.19)$$

Energy equation also discretized using a linear combination of RBFs and is given by equation 4.20.

$$\sum_{j=1}^{N}T_j^{n+1}\phi_j(x_i,y_i)=\sum_{j=1}^{N}T_j^n\phi_j(x_i,y_i)+\Delta t\left[C_T\sum_{j=1}^{N}T_j^n\nabla^2\phi_j(x_i,y_i)-\sum_{j=1}^{N}V_j^n\phi_j(x_i,y_i)\sum_{j=1}^{N}T_j^n\nabla\phi_j(x_i,y_i)\right], \quad (4.20)$$

i = 1,2,……,N_I

where N_I denotes the total number of interior points and N denotes total number of points. Δt denotes the time step, superscript n+1 is the unknown value to be solved, and superscript n is the current known value.

The simulation flow chart is presented in the Figure 4.5. IP and BP in the flow chart represent interior points and boundary points respectively. NC and BFS in the flow chart represent natural convection in a square enclosure and flow over backward facing step.

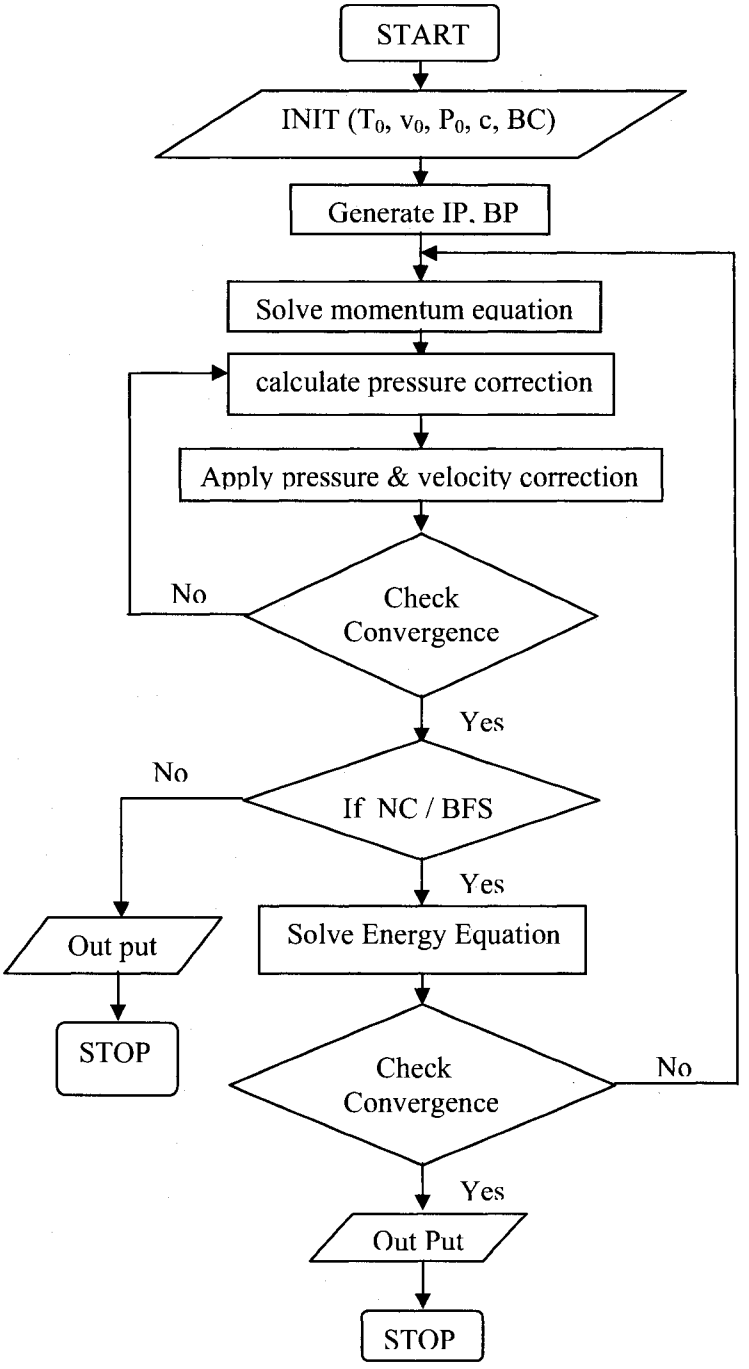

Figure 4.5 Calculation Flow Chart

CHAPTER 5

RESULTS AND DISCUSSION

This thesis explores the use of a simplified RBF approach to calculate coupled heat transfer and fluid flow problems utilizing local pressure correction. The problems addressed include viscous flow in a driven cavity, natural convection in a square enclosure, flow with forced convection over a backward facing step and flow over an airfoil. Results obtained with the present method are compared with results from COMSOL and FLUENT methods. Excellent agreement is achieved compared with results from these two commercial codes.

5.1 Lid-Driven Cavity Flow

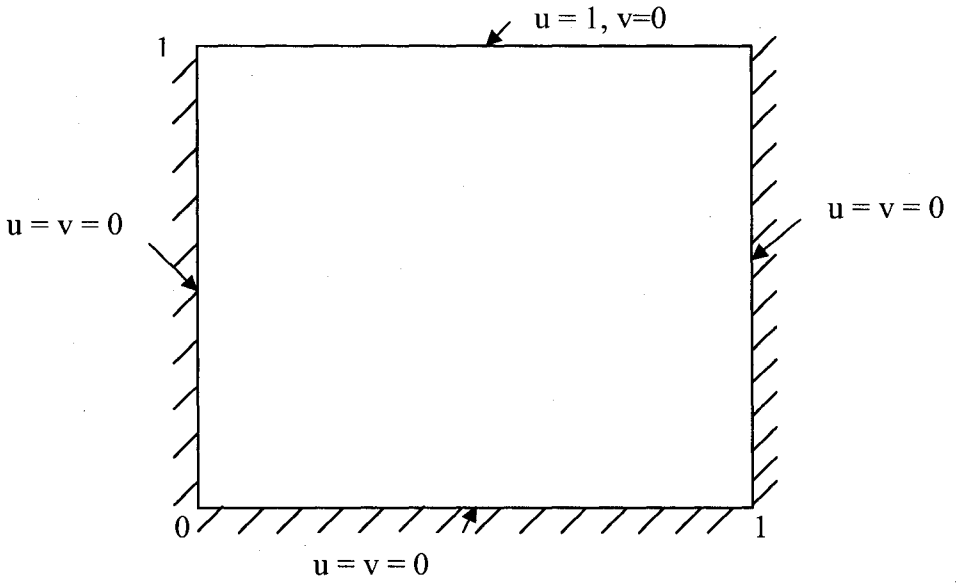

Figure 5.1. Lid driven flow in a square cavity

This is a classical benchmark problem which is suitably used here to demonstrate the capability of the present method to simulate recirculating fluid flows. The computational results for various Reynolds numbers for the lid-driven flow in a square cavity are compared with those obtained by COMSOL and FLUENT. The configuration for this case is shown in Figure 5.1. Uniform point distribution of 31 X 31 is used for RBF approximations. Random point distribution set is also considered to check the accuracy of the method for randomly spaced points. Results obtained are in good agreement with those obtained by uniform point distribution results. Point distributions for 31 X 31 are shown in Figure 5.2.

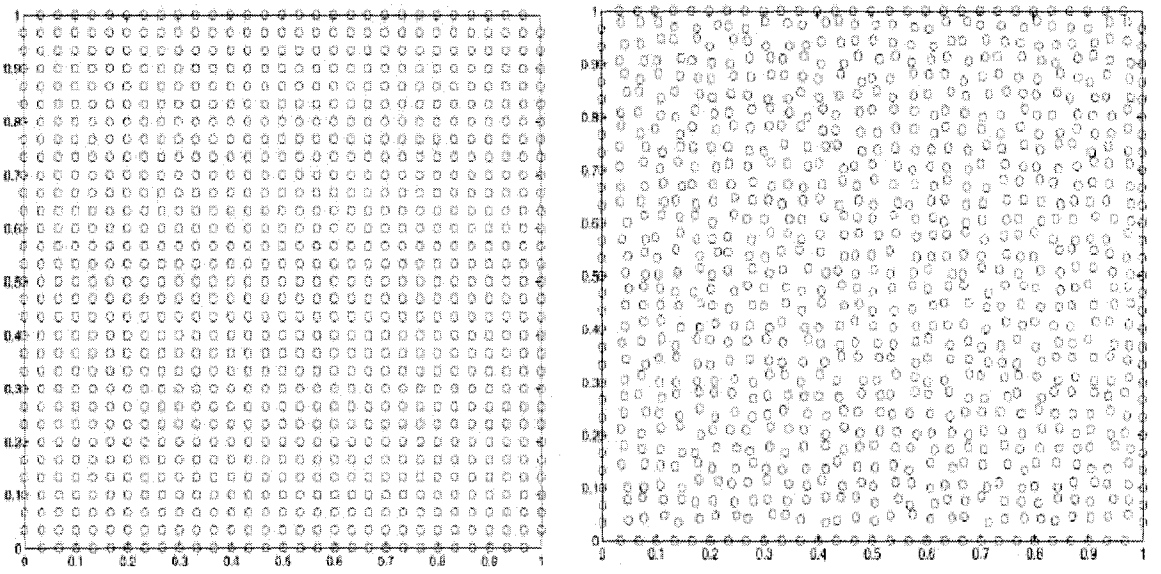

(a) (b)

Figure 5.2. Nodal distributions for lid driven flow (a) Uniform distribution (b) Random distribution

Figure 5.3 compares the velocity profiles at mid-sections of the cavity for 31 X 31 uniform point distribution set and 31 X 31 random point distribution set for Re = 400. Results are in good agreement.

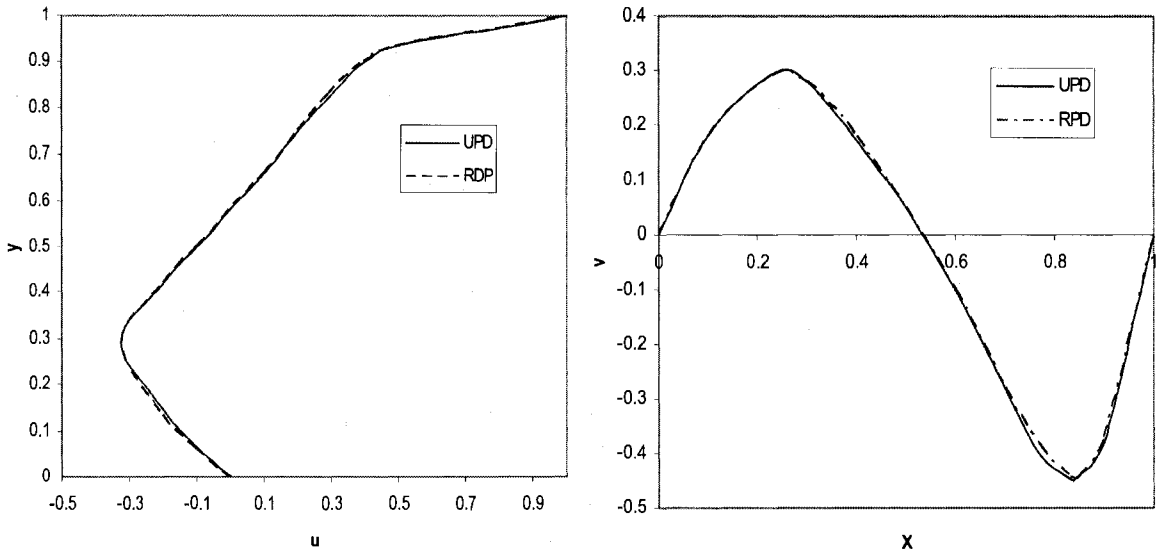

Figure 5.3. velocity profiles for different nodal distributions (Re = 400)

Figure 5.4 shows the meshes used for solving viscous driven flow with COMSOL and FLUENT. Figure 5.5 shows the comparison of velocity vectors in the square cavity for Re = 100 using the meshless method with velocity vectors using COMSOL and FLUENT. The meshless results are in excellent agreement with the two commercial packages.

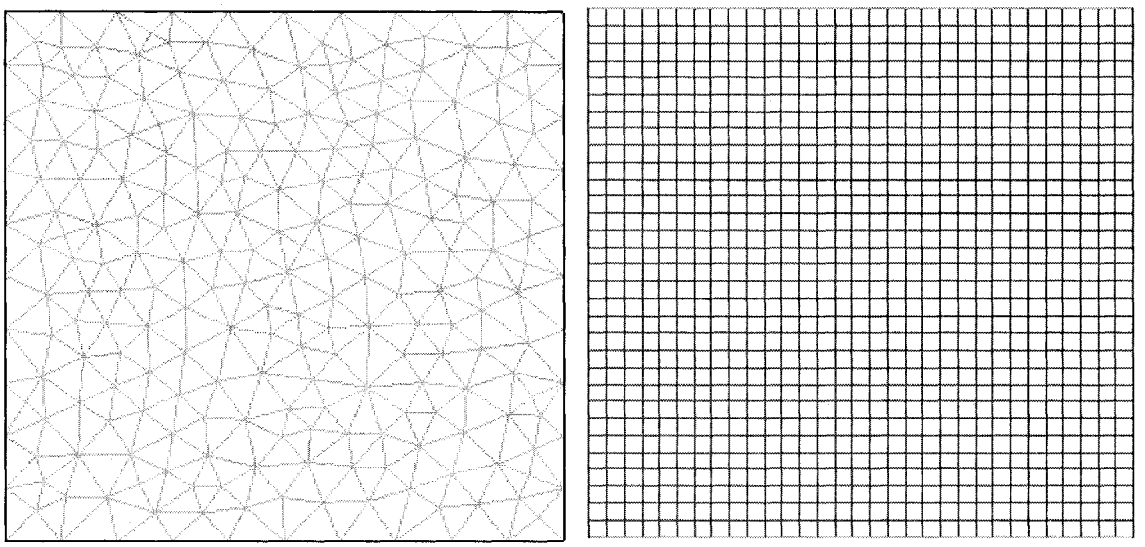

(a) (b)

Figure 5.4. Meshes for lid driven flow (a) COMSOL mesh (1596 nodes)
(b) FLUENT 31 X 31mesh

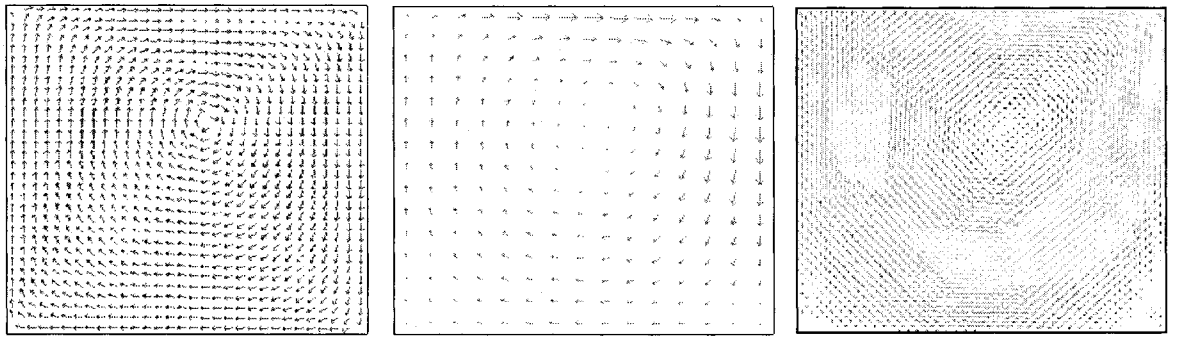

(a) (b) (c)

Figure 5.5. Velocity vectors for flow in a driven cavity using (a) Meshless
(b) COMSOL (c) FLUENT

For the case of Re = 100, velocity profiles on the vertical and horizontal lines through the cavity geometric center are plotted in figure 5.6, and compare well with the corresponding results from COMSOL and FLUENT.

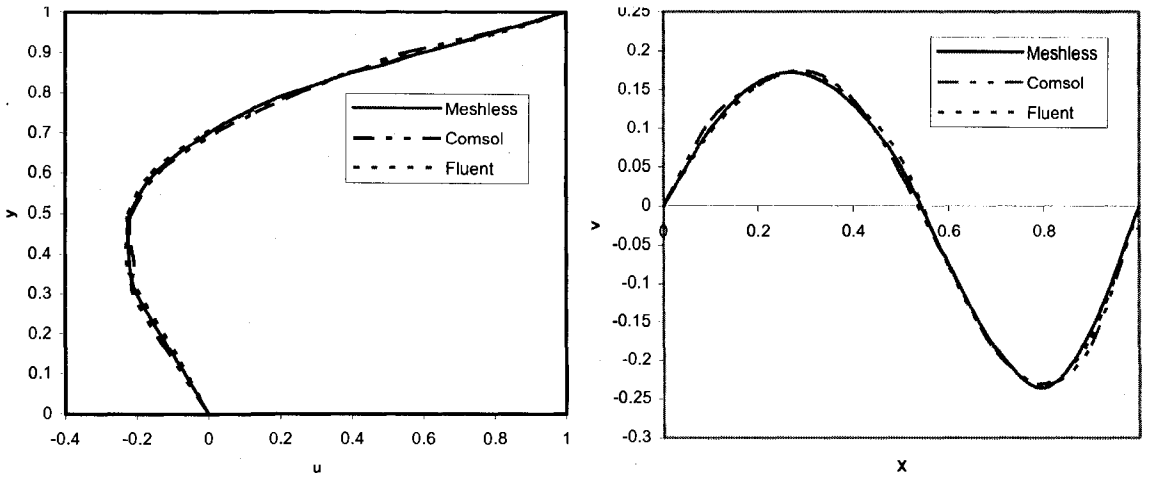

Figure 5.6. Velocity profiles along vertical and horizontal central lines (Re = 100)

For the case of Re = 400, velocity profiles on the vertical and horizontal lines through the cavity geometric center are plotted in figure 5.7.

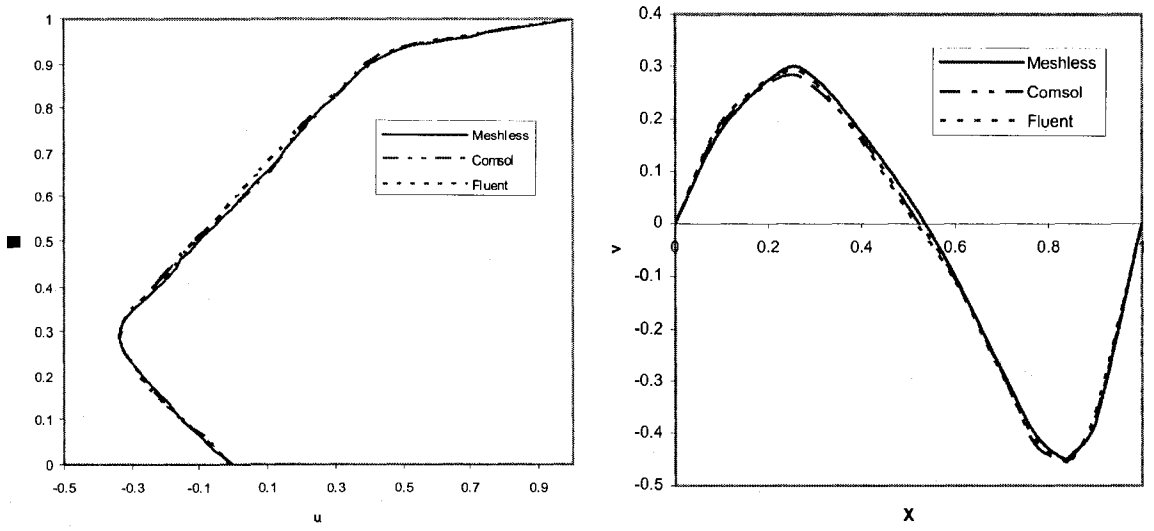

Figure 5.7. Velocity profiles along vertical and horizontal central lines (Re = 400)

For the case of Re = 1000, velocity profiles on the vertical and horizontal lines through the cavity geometric center are plotted in figure 5.8.

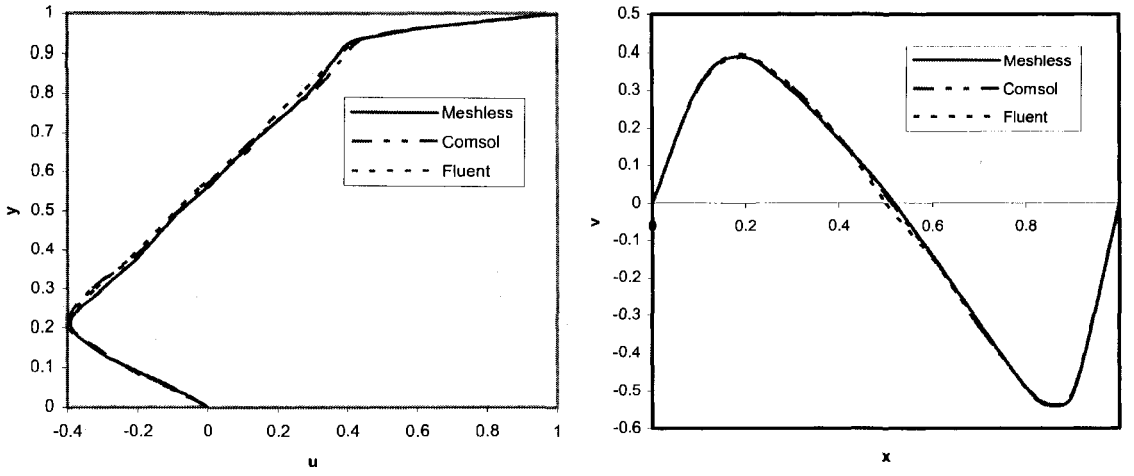

Figure 5.8. Velocity profiles along vertical and horizontal central lines (Re = 1000)

5.2 Natural Convection in a Square Enclosure

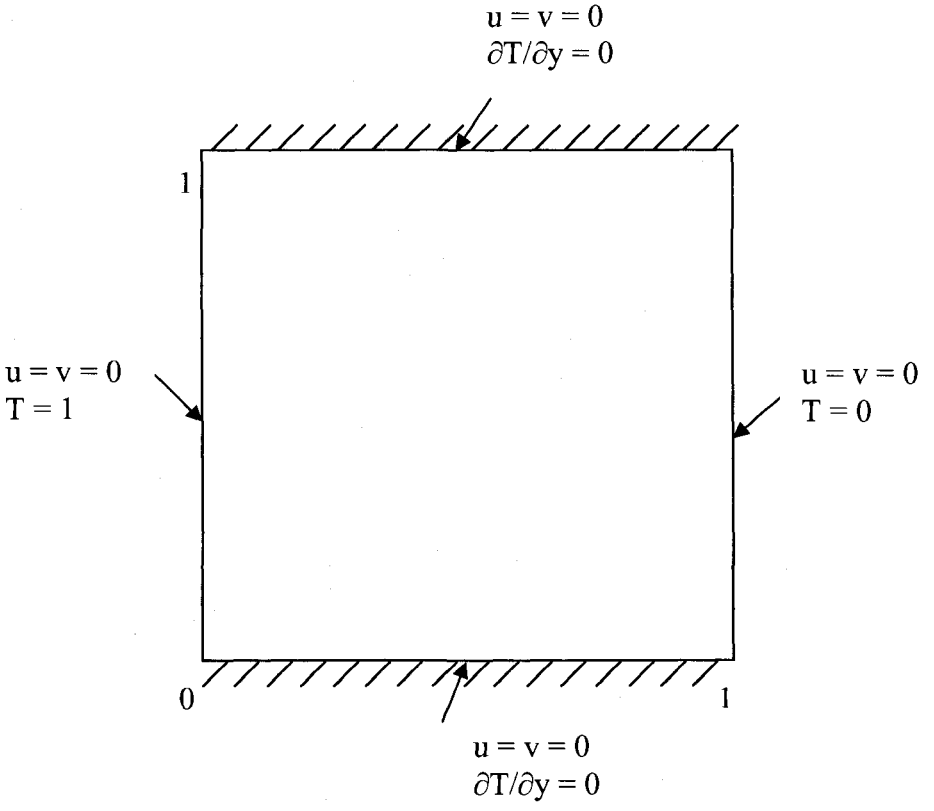

Figure 5.9. Natural convection in a square enclosure

The domain of the problem is a closed square entity filled with air (Prandtl number = 0.71) with differentially heated walls and isolated horizontal walls. With constant initial temperature, pressure and velocity set to zero, steady-state is achieved through time transient. Results for various Rayleigh numbers for the natural convection in a square cavity are compared with those of COMSOL and FLUENT. The configuration of this case is shown in figure 5.9. Distribution of interior nodes and boundary nodes are shown in figure 5.10.

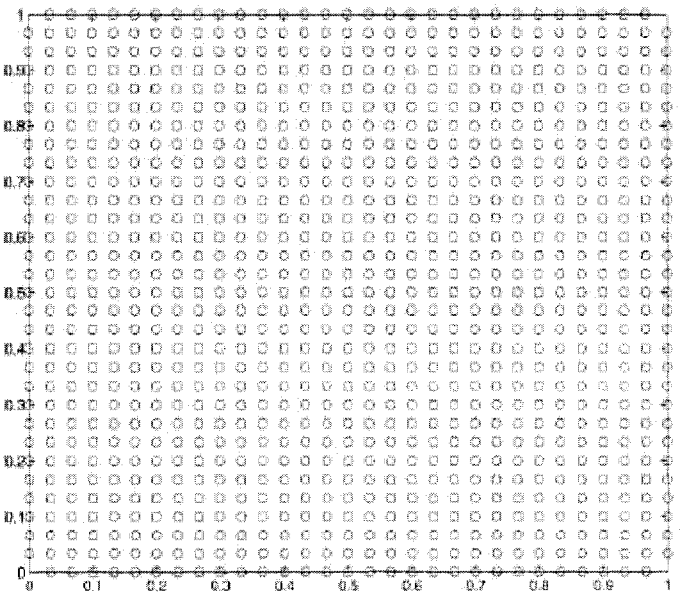

Figure 5.10. Nodal distribution for Natural convection in a square cavity

Figure 5.11 shows the meshes used for solving flow with COMSOL and FLUENT. Figure 5.12 shows the comparison of velocity vectors in the square cavity for Ra = 1000 using the meshless method with velocity vectors using COMSOL and FLUENT. Meshless results are in excellent agreement.

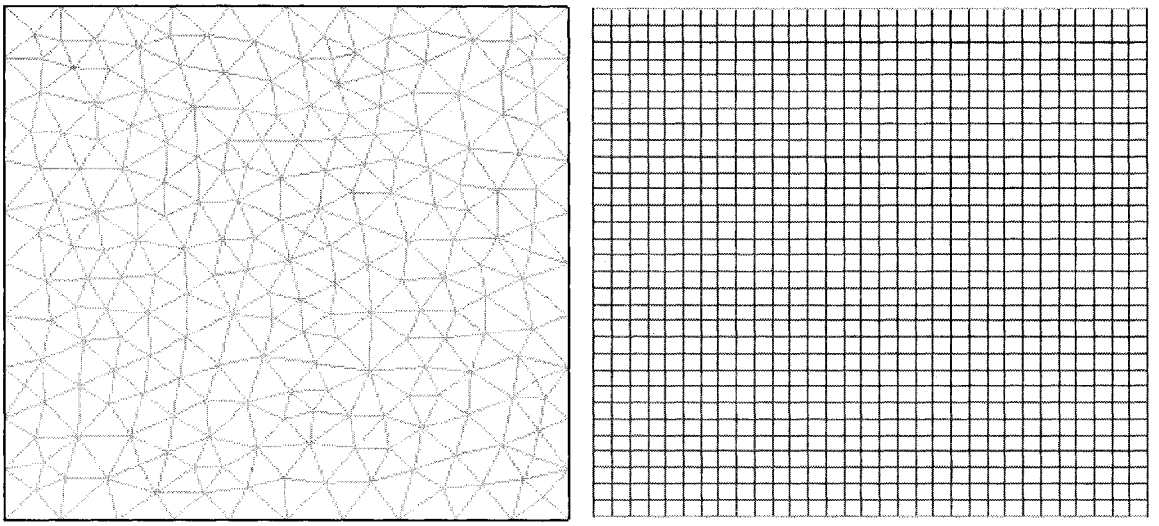

(a) (b)

Figure 5.11. Meshes for Natural Convection (a) COMSOL mesh (1596 nodes) (b) FLUENT 31 X 31 mesh

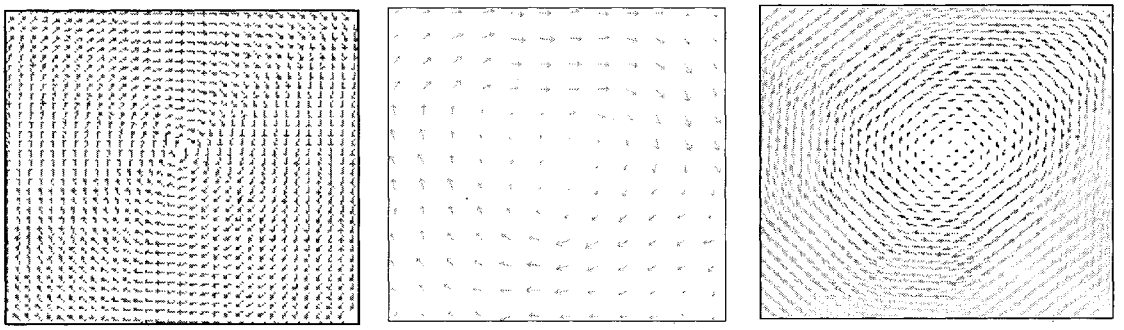

(a) (b) (c)

Figure 5.12. Velocity vectors using (a) Meshless (b) COMSOL (c) FLUENT ($Ra = 10^3$)

For the case of $Ra = 10^3$, velocity profiles on the vertical and horizontal lines through the cavity geometric centre are plotted in Figure 5.13 and compare closely with the corresponding results from COMSOL and FLUENT.

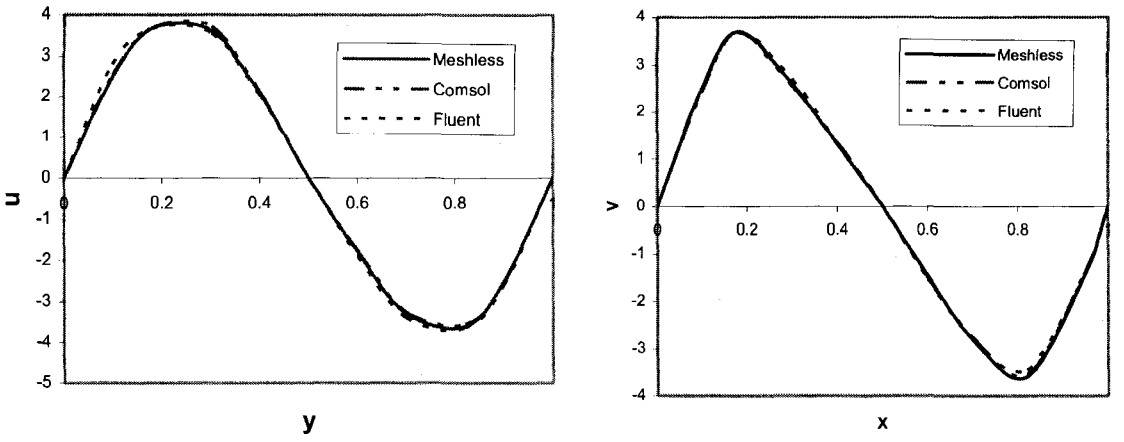

Figure 5.13. Velocity profiles along vertical and horizontal central lines (Ra = 10^3)

For the case of Ra = 10^4, velocity profiles on the vertical and horizontal lines through the cavity geometric center are shown in figure 5.14.

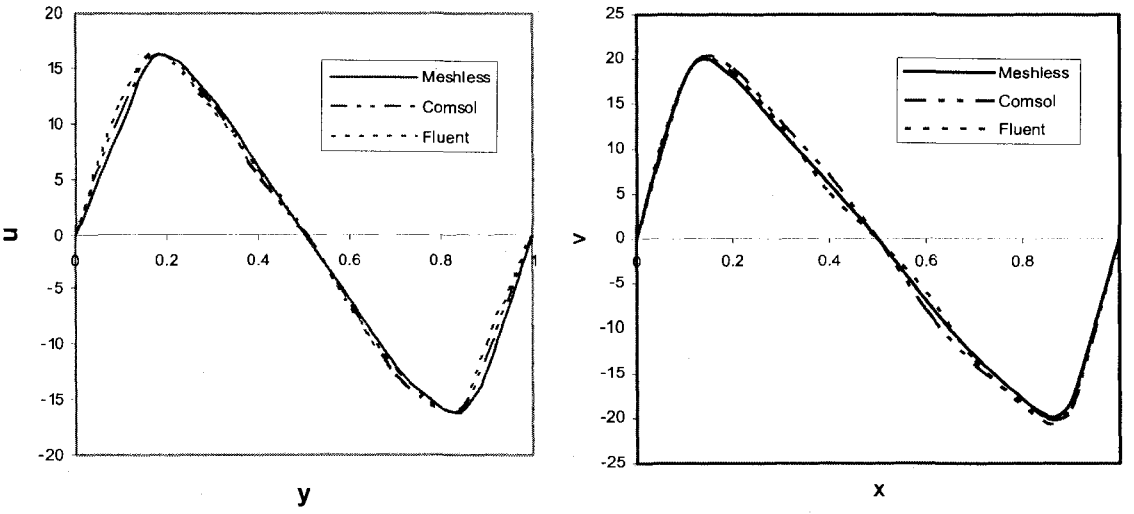

Figure 5.14. Velocity profiles along vertical and horizontal central lines (Ra = 10^4)

For the case of Ra = 10^5, velocity profiles on the vertical and horizontal lines through the cavity geometric center are shown in figure 5.15.

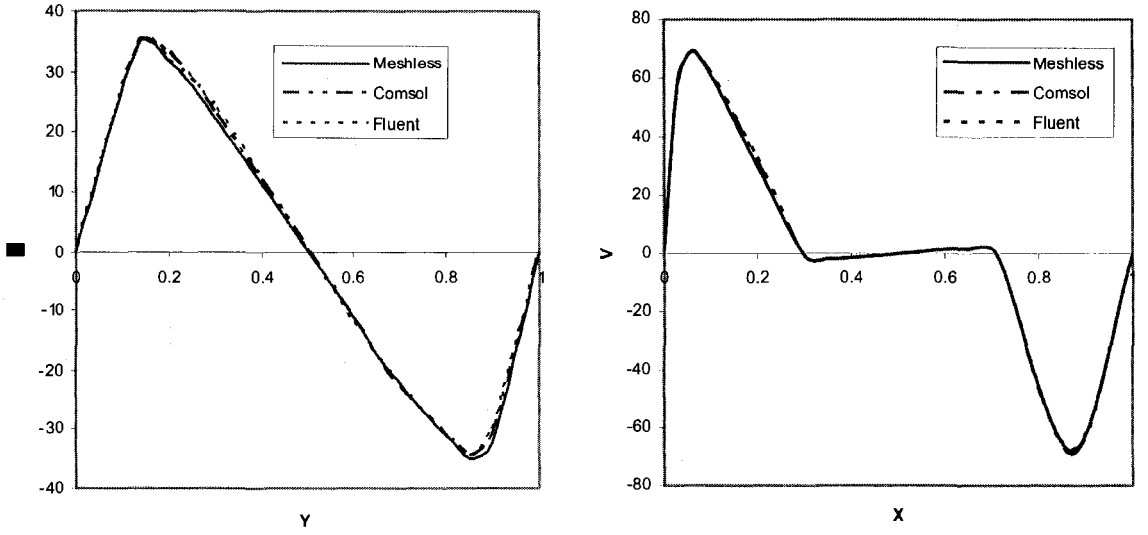

Figure 5.15. Velocity profiles along vertical and horizontal central lines (Ra = 10^5)

In figure 5.16 simulation results of the temperature contours ranging from 0 to 1 with 0.1 as the interval for Ra = 10^4 are compared with results of COMSOL and FLUENT. Meshless results are again in excellent agreement.

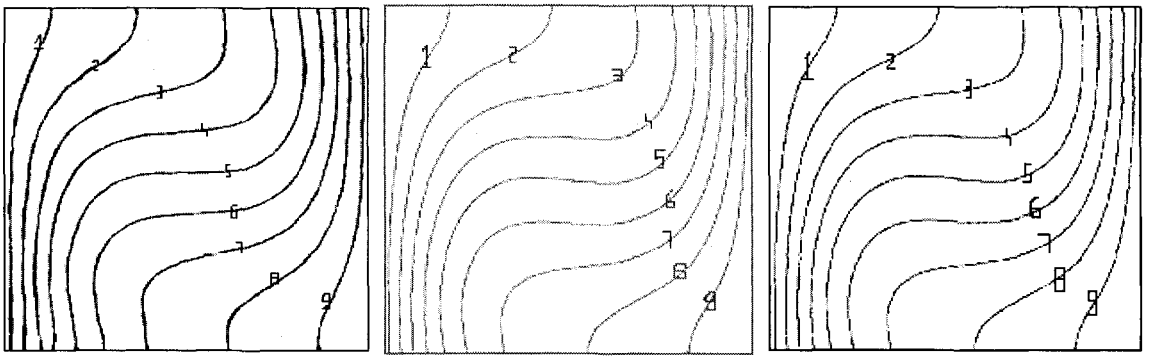

(a) (b) (c)

Figure 5.16. Isotherms for Natural convection in a square cavity for Ra = 10^4 using (a) Meshless (b) COMSOL (c) FLUENT

Simulation results of the temperature contours from 0 to 1 with 0.1 as interval for $Ra = 10^4$ are compared with results of COMSOL and Fluent In Fig. 5.16.

5.3 Flow with Forced Convection over Backward Facing Step

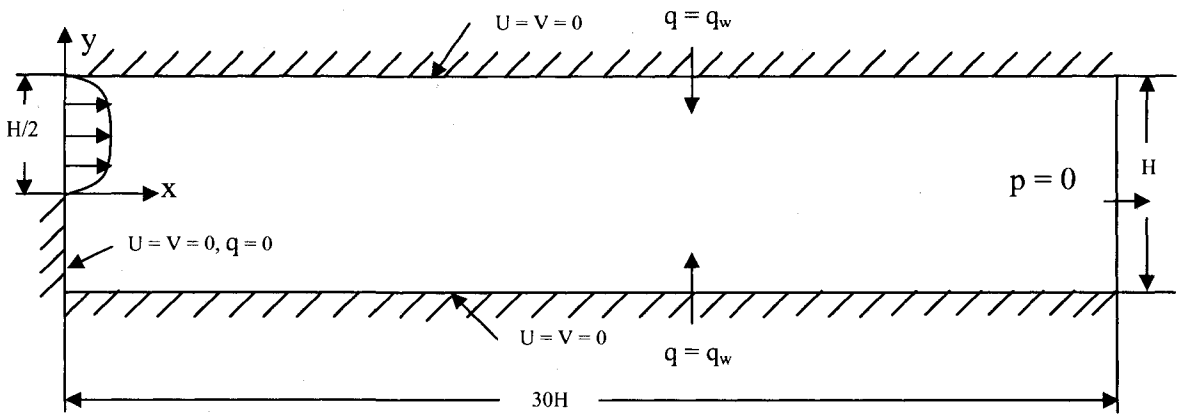

Figure 5.17. Problem configuration for flow over backward facing step

Figure 5.17 shows the configuration of forced convection over the 2-D backward facing step. A constant heat flux is introduced into the upper and lower channel walls immediately downstream of the step. The purpose of this particular set of conditions is to evaluate the change in temperature along the upper and lower surfaces as initially heated flow proceeds down the channel. Ideally, the temperature gradient approaches a constant value with increasing horizontal distance from the step. Flow over the two-dimensional backward facing step is simulated for Re=800 and Pr=0.71. Distribution of interior nodes and boundary nodes are shown in Fig. 5.18.

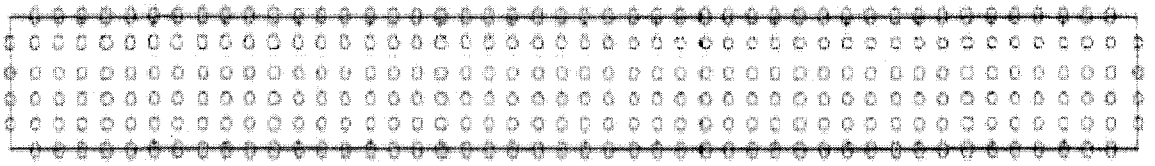

Figure 5.18. Distribution of 284 nodes for flow over backward facing step

Figure 5.19 shows the meshes obtained using COMSOL and FLUENT. Figure 5.20 shows the comparison of velocity vectors over the backward facing step for Re = 800. The meshless results again are in excellent agreement.

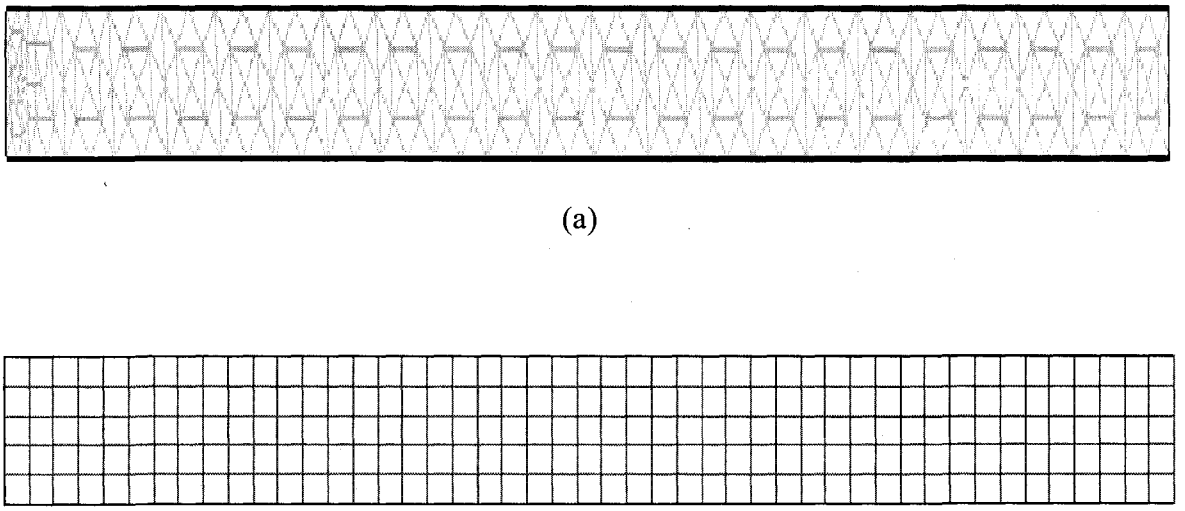

(a)

(b)

Figure 5.19. Meshes for backward facing step solution (a) COMSOL mesh of 388 elements (b) FLUENT mesh of 284 nodes

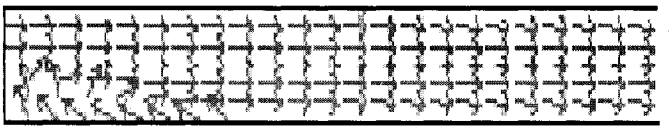

(a)

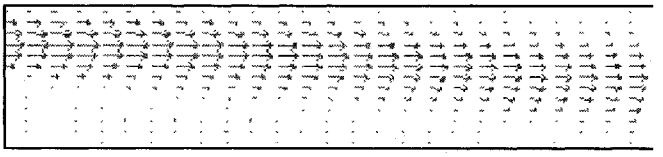

(b)

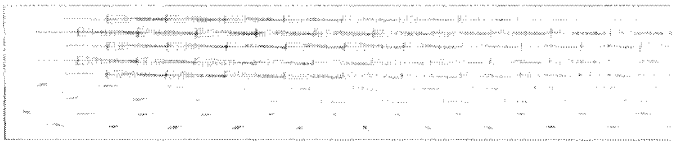

(c)

Figure 5.20. Velocity vectors for backward facing step using (a) Meshless (b) COMSOL (c) FLUENT

Velocity profiles at x = 7 and at x = 15 are shown in Fig. 5.21 and Fig. 5.22. Present results compare closely with those obtained by COMSOL and FLUENT.

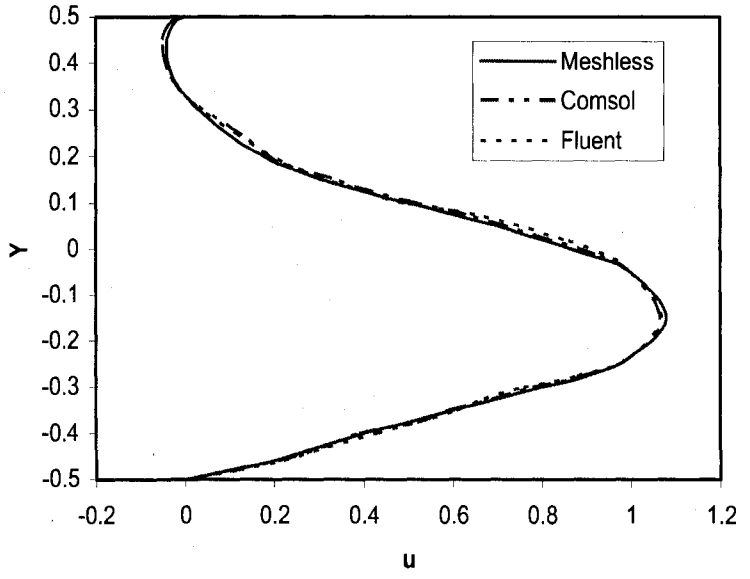

Figure 5.21. Velocity profile for Re = 800 at x = 7

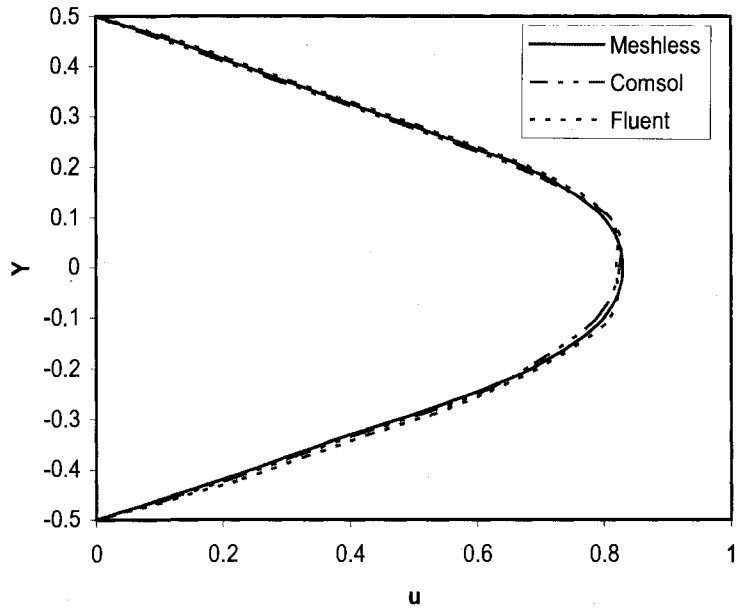

Figure 5.22. Velocity profile for Re = 800 at x = 15

Temperature profiles at x = 7 and at x = 15 are shown in figure 5.23 and figure 5.24, respectively. A comparison of temperature show excellent agreement.

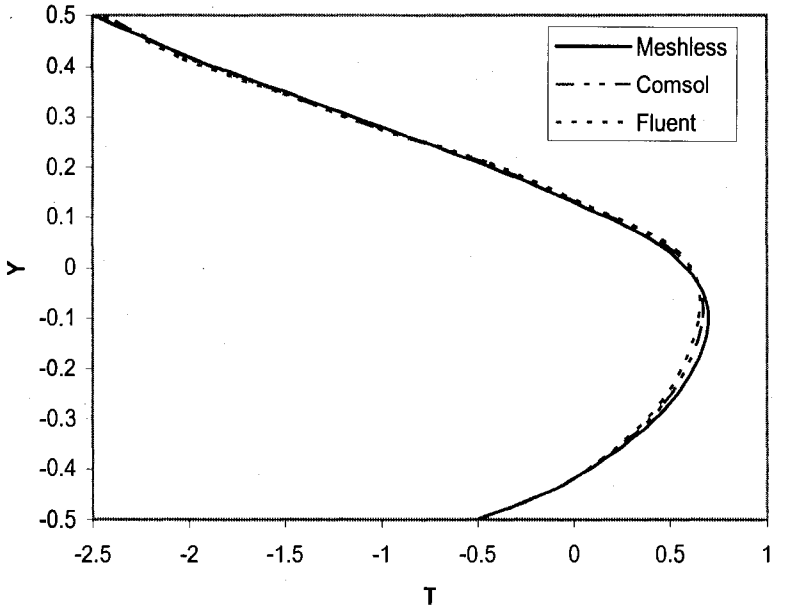

Figure 5.23. Temperature profile for Re = 800 at x = 7

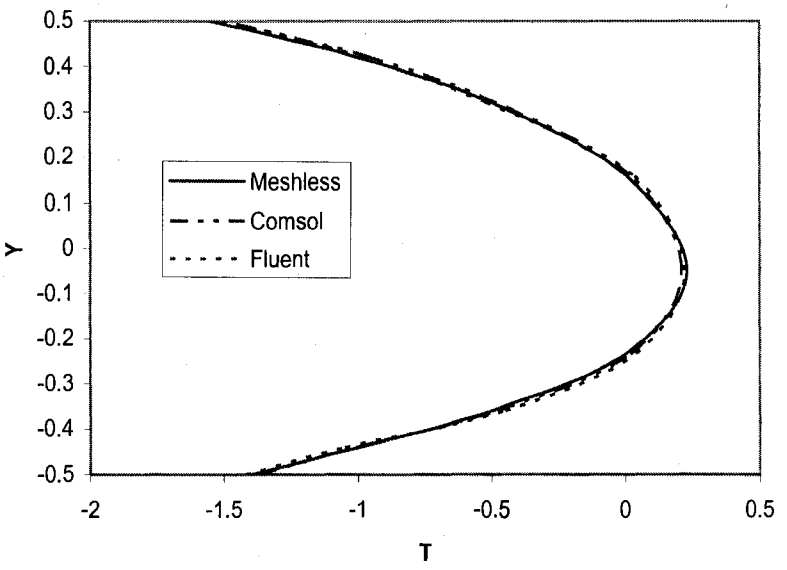

Figure 5.24. Temperature profile for Re = 800 at x = 15

Temperature contours for Re = 800 are shown in figure 5.25. The isotherms are nearly identical for all three models.

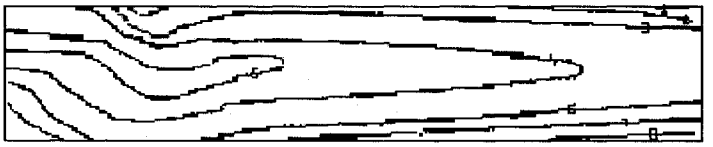

(a)

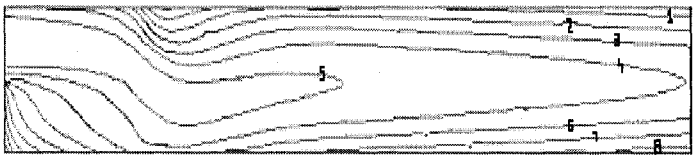

(b)

(c)

Figure 5.25. Isotherms for backward step flow using (a) Meshless (b) COMSOL (c) FLUENT

5.4 Flow over an airfoil

Figure 5.26 shows the configuration of flow over an airfoil in a rectangular domain. A Selig S1210 which is a high lift, low Reynolds number airfoil with zero attack angle is examined.

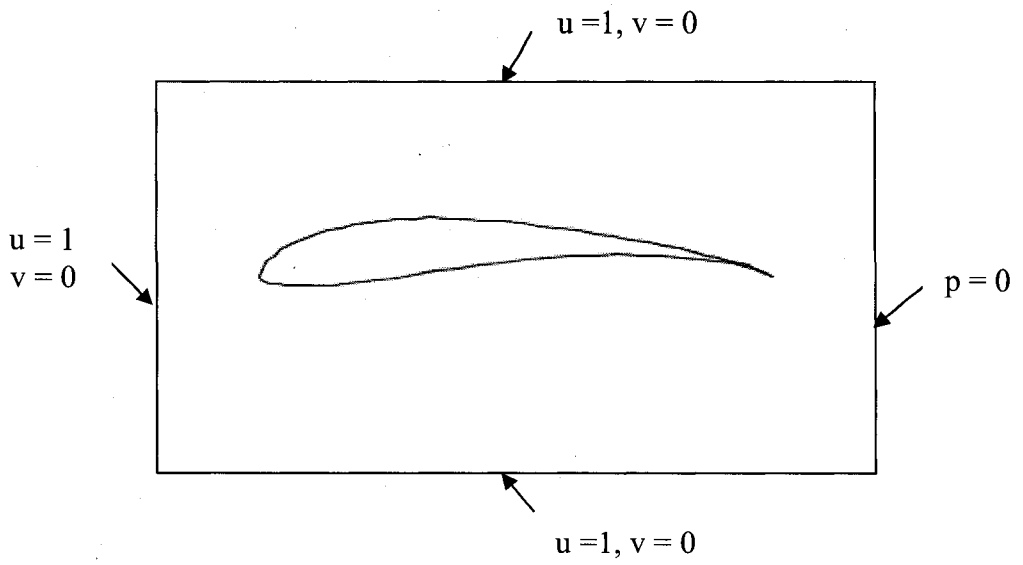

Figure 5.26. Problem configuration for flow over an airfoil

Figure 5.26 shows the configuration of flow over an airfoil in a rectangular domain. A Selig S1210 which is a high lift, low Reynolds number airfoil with zero attack angle is examined. Several studies employed systematic experiments and others employed various numerical schemes [49-50]. Distribution of interior nodes and boundary nodes are shown in figure 5.27.

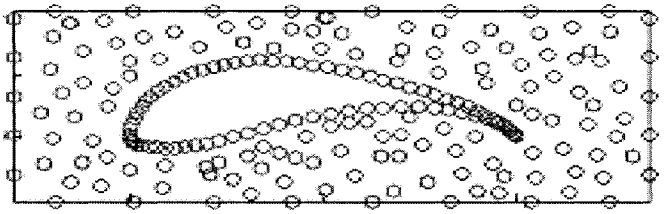

Figure 5.27. Distribution of 236 nodes in a rectangular domain

Figure 5.28 shows the meshes used for solving the flow with COMSOL and FLUENT. Figure 5.29 shows the comparison of velocity vectors for Re = 300.

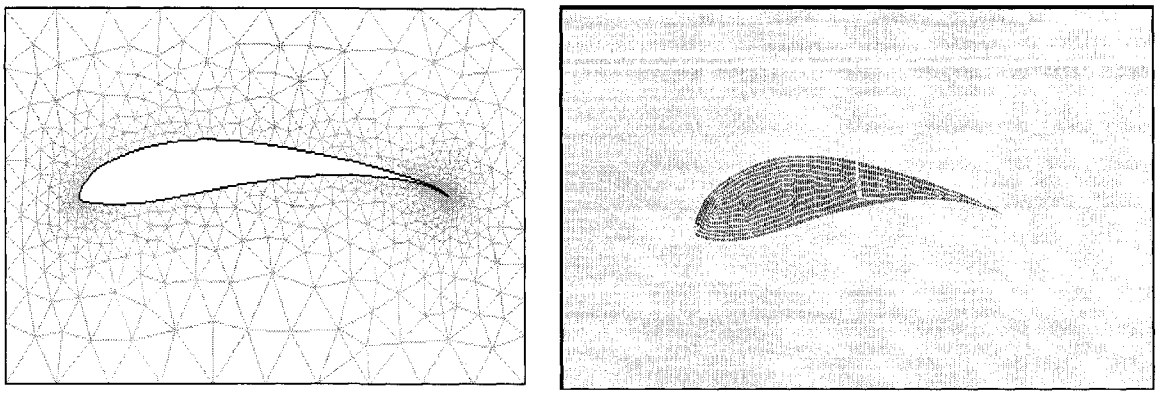

(a) (b)

Figure 5.28. Meshes for flow over an airfoil (a) COMSOL mesh of 2535 elements (b) FLUENT mesh of 1893 nodes

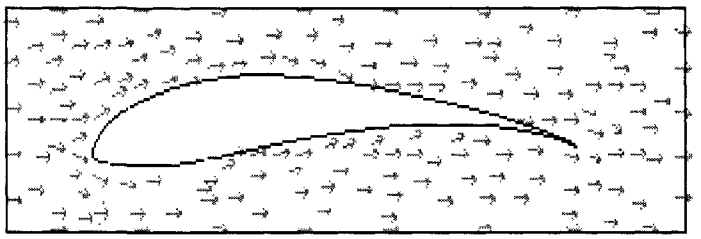

(a)

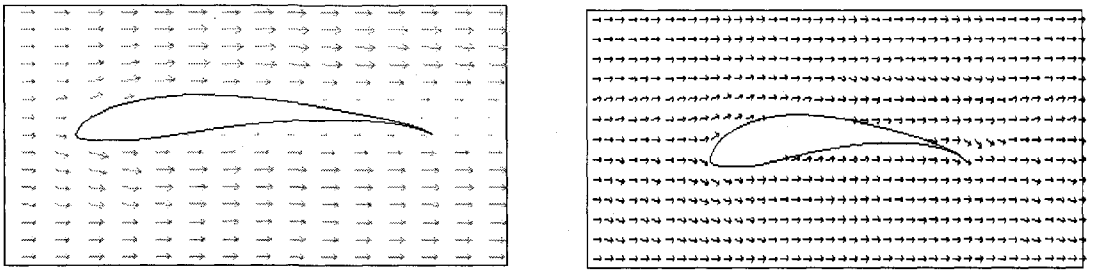

(b) (c)

Figure 5.29. Velocity vectors for flow over an airfoil using (a) Meshless (b) COMSOL (c) FLUENT

CHAPTER 6

CONCLUSIONS AND FUTURE WORK

6.1 Conclusions

For complex geometries the process of grid generation can be quite time consuming and cumbersome. Researchers have shown interest in a class of methods known as meshless methods which do not require any kind of mesh to be generated to solve the governing equations. In the present work an attempt has been made to develop a computational technique based on meshless methods. The present scheme can work on a random or uniformly distributed set of nodes. These nodes do not need to be related, nor does connectivity information need to be stored.

Radial basis functions (RBFs) are used as basis functions to approximate a function and its derivatives. In this study, lid-driven cavity flow, natural convection in a square enclosure, flow with forced convection over a backward facing step and flow over an airfoil were solved. Results are compared with the benchmark solutions. From the comparisons made, it can be seen that the meshless method is effective in solving the incompressible Navier-Stokes equations. The number of points required to obtain comparable accuracy is much less than mesh-based methods, and appears to be a viable alternative method for solving fluid flow and heat transfer problems.

This thesis explores the simplified RBF approach for the calculation of the coupled heat transfer and fluid flow using a local pressure correction scheme. The algorithm is very simple to numerically implement, fast and robust.

Numerical implementation was done in MATLAB. Using only a one step pressure correction, the algorithm needs only a small number of calculations per iteration cycle. The combined procedure makes the algorithm fast and robust. Excellent agreement was achieved using model results obtained by COMSOL and FLUENT.

6.1 Future work

Meshless methods are still an area where much research is required to standardize the methods, improve their accuracy and efficiency. Most meshless methods suffer from common problems such as low order accuracy, ill-conditioned matrices, and slow computational speed when compared to conventional methods. Few researchers have attempted to address the aforementioned problems.

One of the important factors which determine the accuracy in any node based meshless solver is the node distribution. Node generation techniques in meshless methods vary from problem to problem. Some research has been devoted to algorithms for node generation with optimum node density for meshless solvers. These node generation techniques can generate appropriate node density depending on the problem under consideration.

There are numerous algorithms for choosing the right shape parameter c for best approximation using RBFs. However, there is no theoretical study that has addressed the influence of shape parameter on accuracy. Many meshless methods are computationally

inefficient when compared to present day FDM/FVM/FEM techniques. Better search algorithms can be used to improve the computational speed and efficiency of meshless methods in general and radial basis function based meshless methods in particular.

Further work should be focused on more complex geometric situations and more complex physical models (porous media, solidification,….). These problems should be relatively easy to numerically implement in the present context.

REFERENCES

1 Atluri, S.N. and Shen, S. (2002), "The meshless local Petrov-Galerking (MLPG) method: a simple & less-costly alternative to the finite element and boundary element method", Computer Modelling in Engineering & Sciences, Vol. 3, pp. 11-52.

2 Chen, W. (2002), "New RBF collocation schemes and kernel RBFs with applications", Lecture Notes in Computational Science and Engineering, Vol. 26, pp. 75-86.

3 Kansa, E.J (1990), "Multiquadrics – a scattered data approximation scheme with application to computational fluid dynamics, part I", Computers and Mathematics with Applications, Vol. 19, pp. 127-145.

4 Sarler, B and Kuhn, G. (1999), "Primitive variables dual reciprocity boundary element method solution of incompressible Navier-Stokes equations", Engineering Analysis with Boundary Elements, Vol. 23, pp. 443-455.

5 Sarler, B. (2002), "Towards a mesh-free computation of transport phenomena", Engineering Analysis with Boundary Elements, Vol. 26, pp. 731-738.

6 Lin, H. and Atluri, S.N. (2001), "Meshless local Petrov Galerkin Method (MLPG) for convection-diffusion problems", Computer Modelling in Engineering and Sciences, Vol. 1, pp. 45-60.

7 Buhman, M.D. (2000), Radial Basis Functions, Cambridge University Press, Cambridge.

8 Lewis, R.W., Morga, K., Thomas, H.R. and Seetharamu, K.N. (1996), "The Finite element method in Heat Transfer Analysis", J. Wiley & Sons: Chichester, UK.

9 Huang, H.C. and Usmani, A.S. (1994), "Finite Element Analysis for Heat Transfer", Springer-Verlag: London, UK.

10 Liu, G.R. (2002), "Mesh Free Methods: Moving Beyond the Finite Element Method", CRC Press, Boca Raton, FL.

11 Lucy, L.B. (1977), "A Numerical approach to the testing of the fission hypothesis", The Aston. J., Vol 8(12), pp. 1013-1024.

12 Atluri, S.N., Kim, H.K. and Cho, J.Y.(1999), "A critical assessment of the truly meshless local Petrov-Galerkin (MLPG), and local boundary integral equation (LBIE) methods", Computational Mechanics, Vol.24, pp. 348-372.

13 La-Rocca, A., Power, H., La-Rocca, V. And Morale, M. (2005), " A meshless approach based upon radial basis function hermite collocation method for predicting the cooling and the freezing times of foods", CMC: Computers, Materials & Continua, vol. 2, pp. 239-250.

14 Mai-Duy, N. (2004), "Indirect RBFN method with scattered points for numerical solution of PDEs.", CMES: Computer Modeling in Engineering & Sciences, vol. 6, pp. 209-226.

15 Hon, Y., Ling, L. and Liew, K. (2005), "Numerical analysis of parameters in a laminated bean model by radial basis functions", CMC: Computers, Materials & Continua, vol.2, pp. 39-50.

16 Mai-Duy, N. (2001), "Numerical solution of differential equations using multiquadric radial basis function networks",Neural Networks,vol.14, pp.185-199.

17 Mai-Duy, N. and Tran-Cong, T. (2005), "An efficient indirect RBFN-based method for numerical solution of PDEs", Numerical Methods for Partial Differential Equations, vol. 21, pp. 770-790.

18 Belytschko, T., Kronganz, Y. and Organ, D. (1996), "Meshless methods: An overview and recent developments", Comput. Methods Appl. Mech. Enrg., vol. 139, pp. 3-47.

19 Larsson, E., Fornberg. B. (2003), "A numerical study of some radial basis function based solution method for elliptic PDEs", Computers and Mathematics with Applications, vol. 46, pp. 891-902.

20 Shu, C., Ding, H., Chen, H.Q., and Wang, T.G. (2001), "An upwind local RBF-DQ method for simulation of inviscid compressible flows", Comput. Methods Appl. Mech. Engrg., vol 194, pp. 2001-2017.

21 Ramachandran, P. and Balakrishnan, K., "Radial basis functions as approximate particular solutions: review of recent progress", Engineering Analysis with Boundary Elements, vol. 24, pp. 575-582.

22 Ding, H., Shu, C., Yeo, K.S. and Xu, D. (2004), "Development of least square based two dimensional finite difference schemes and their application to simulate natural convection in a cavity", Computers and Fluids, vol. 33, pp. 137-154.

23 Armin, B. and Holger, W. (2001), "Multivariate interpolation for fluid structure interaction problems using radial basis functions", Aerospace science and technology, vol. 5, pp. 125-134.

24 Sarler, B., Perko, J. and Chen, C.S. (2004), "Radial basis function collocation method solution of natural convection in porous Media", International Journal of Numerical Methods for Heat & Fluid Flow, vol. 14, pp. 187-212.

25 Divo, E. and Kassab, A.J. (2007), "An efficient localized RBF meshless method for fluid flow and conjugate heat transfer", ASME journal of Heat Transfer, Vol. 129, pp. 124-136.

26 Davis, G. and De Vahl (1983), "Natural convection of air in a square cavity: a bench mark numerical solution", International Journal of Numerical Methods in Fluids, Vol. 3, pp. 249-264.

27 Sarler, B. (2005), "A radial basis function collocation approach in computational fluid dynamics", Computer Modeling in Engineering & Sciences, vol.7, pp. 185-193.

28 Vertnik, R. and Sarler, B. (2006), "Meshfree Explicit Local Radial Basis Function Collocation Method for Diffusion Problems", Computer and Mathematics with Applications, vol. 51, pp. 1269-1282.

29 Sarler, B. and Vertnik, R. (2006), "Meshfree Explicit Local Radial Basis Function Collocation Method for Convective and Diffusive solid-liquid phase-change problems", International Journal of Numerical Methods for Heat and Fluid Flow, vol. 16, pp. 961-5539.

30 Vertnik, R., Zaloznic, M. and Sarler, B. (2006), "Solution of transient direct – chill aluminium billet casting problem with simultaneous material and interface moving boundaries by a meshless method", Engineering Analysis with Boundary Elements, vol. 30, pp. 847-855.

31 Schaback, R., (1995) "Error estimates and condition numbers for radial basis function interpolants", Adv. Comput. Math., vol. 3, pp. 251-264.

32 Narcowich, F.J. and Ward, J.D., (1992), " Norm estimates for the inverses of a general class of scattered-data radial-function interpolantion matrices", J. Approx. Theory, vol. 69, pp. 84-109.

33 Hardy, R.L., (1971), "Multiquadric equations of topography and other irregular surfaces", J. Geophy. Res., vol. 76, pp. 1905-1915.

34 Franke, R. (1979), "A critical comparison of some methods for interpolation of scattered data", TR NPS-53-79-003, Naval Postgraduate School.

35 Micchelli, C.A., (1986), "Interpolation of scattered data: distance matrices and conditionally positive definite functions", Constr. Approx., vol. 2, pp. 11-22

36 Franke, C., Schaback R. (1998), "Solving partial differential equations using radial basis functions", Applied mathematics and computations, vol. 3, pp. 73-82.

37 Wang, J.G. and Liu, G.R. (2002), "On the optimal shape parameter of radial basis functions used for 2-D meshless methods", Comput. Methods Appl. Mech. Engrg,vol. 91, pp. 2611-2630.

38 Koseff, J.R. and Street, R.L. (1984), "Visualization studies of a Shear Driven Three Dimensional Recirculation Flow", J. Fluids Eng., vol. 106, no.1, pp. 21-29.

39 Koseff, J.R. and Street, R.L. (1984), "On end wall effects in a lid-driven cavity flow", J. Fluids Eng., vol. 106, no. 4, pp. 390-398.

40 Koseff, J.R. and Street, R.L. (1984), "Lid-driven cavity flow: A synthesis of qualitative and quantitative observations", J. Fluids Eng., vol. 106, no. 4, pp. 385-389.

41 Ghia, U., Ghia, K.N. and Shin,C.T. (1982), " High-Re solutions for incompressible flow using the Navier-Stokes equations and a multigrid method", J. Comp. Phys., vol. 48, pp. 387-411.

42 Jiang, B.N., Lin, T.L. and Povinelli, L.A. (1994), " Large-scale computation of incompressible viscous flow by least-squares finite element method", Comput. Meth. Appl. Mech. Eng., vol. 114, pp. 213-231.

43 Gresho, P.M. (1984), "A modified Finite Element method for solving the time-dependent incompressible Navier-Stokes Equations", Part 2: Applications, Int. J. Numer. Meth. Fluids, vol.4, pp. 619-640.

44 Shu, C. and Wee, K.H.A (2002), "Numerical simulation of natural convection in a square cavity by simple-generated differential quadrature method", Computers & Fluids, vol. 31, pp. 209 – 226.

45 Tian, Z.F. and Ge. Y.B. (2003), "A fourth-order compact finite difference scheme for the steady stream function-vorticity formulation of the navier-stokes/boussinesq equations", Int. J. Numer. Meth. Fluids, Vol. 41, pp. 495-518.

46 Wansophark, N. and Dechaumphai, P. (2004), "Combined adaptive meshing technique and segregated finite element algorithm for analysis of free and forced convection heat transfer", Finite element analysis and design, vol. 40, pp. 645-663.

47 Niu, J. and Zhu, Z. (2004), "Numerical evaluation of weakly turbulent flow patterns of natural convection in a square enclosure with differentially heated side walls", Numer. Heat Transfer, vol. 45, pp. 551-568.

48 De Vahl Davis, G. (1983), "Natural convection of air in a square cavity: A bench mark numerical solution", Int. J. Numer. Meth. Fluids, vol. 3, pp. 249-264.

49 Shur, M., Spalart, P.R., Strelets, M., and Travin, A. (1999), "Detached-eddy simulation of an airfoil at high angle of attack", 4th Int. Symp. Eng. Turb. Modelling and Measurements, Corsica, May 24-26.

50 Rupesh, B. Kotapati-Apparao and Kyle D. Squires (2004), "Prediction of flow over an airfoil at maximum lift", Aerospace Science Meeting, Jan 5-8.

51 Gartling, D.K. (1990), "A Test Problem for Outflow Boundary Conditions – Flow over a Backward-Facing Step", Int. J. Numer. Meth. Fluids, vol. 11, pp. 953-967.

52 Blackwell, B.F. and Pepper, D.W. (1992), "Benchmark Problems for Heat Transfer Codes, HTD", vol. 21, pp. 190-198.

VITA

Graduate College
University of Nevada Las Vegas

Nagamani Devi Kalla

Address:
4759 Crakow Ct.
Las Vegas, NV – 89147

Degree:

- Bachelor of Engineering, Mechanical Engineering, 2001
  Nagarjuna University, India

Work Experience:

- Worked as Project Fellow in National Metallurgical Laboratory, India for two years

Publications:

- Nagamani Devi Kalla, D.W. Pepper, "*A Meshless Radial Basis Function Method for Fluid Flow with Heat Transfer*", ICCES, vol. 142, no.1, pp. 1-6, 2008.

Thesis Title: Solution of Heat Transfer and Fluid Flow Problems using Meshless Radial Basis Function Method

Thesis Examination Committee:
Chairperson, Dr. Darrell Pepper, Ph.D.
Committee Member, Dr. William Culbreth, Ph.D.
Committee Member, Dr. Daniel Cook, Ph.D.
Graduate College Representative, Dr. Rama Venkat, Ph.D.